Gou Sanhu (Orcid ID: 0000-0003-3231-7427)

A novel apoA-I mimetic peptide suppresses atherosclerosis by promoting physiological HDL function in apoE$^{-/-}$ mice

Running title: Novel apoA-I mimetic peptide suppresses atherosclerosis in mice

Sanhu Gou[1], Li Wang[1], Chao Zhong[1, 2], Xinyue Chen[1], Xu Ouyang[1], Beibei Li[1], Guangjun Bao[3], Hui Liu[1], Yun Zhang[1], Jingman Ni[1]

[1]Institute of Pharmaceutics, School of Pharmacy, Lanzhou University, Lanzhou P.R. China

[2]Key Laboratory of Preclinical Study for New Drugs of Gansu Province, School of Basic Medical Sciences, Lanzhou University, Lanzhou P.R. China

[3]Institute of Biochemistry and Molecular Biology, School of Life Sciences, Lanzhou

Correspondence

Jingman Ni, PhD, Professor, Institute of Pharmaceutics, School of Pharmacy, Lanzhou University, 222 Tianshui South Road, Lanzhou, 730000, P.R. China.

Email: nijm@lzu.edu.cn

This article has been accepted for publication and undergone full peer review but has not been through the copyediting, typesetting, pagination and proofreading process which may lead to differences between this version and the Version of Record. Please cite this article as doi: 10.1111/bph.15213

Funding information

National Natural Science Foundation of China, Grant/Award Number: 81273440, 81773564.

Word count (excluding figure legends and references): 7037

Abstract:

Background and Purpose: Apolipoprotein A-I (apoA-I) mimetic peptides (AMPs) are short peptides that can mimic the physiological effects of apoA-I, including the suppression of atherosclerosis by reversely transporting peripheral cholesterol to the liver. As the hydrophobicity of apoA-I is considered important for its lipid transport, novel AMPs were designed and synthesized in this study by gradually increasing the hydrophobicity of the parent peptide and their anti-atherosclerotic effects were tested.

Experimental Approach: Seventeen new AMPs (P1–P17) with incrementally increased hydrophobicity were designed and synthesized by replacing the amino acids 221–240 of apoA-I (VLESFKVSFLSALEEYTKKL). Their effects on cholesterol efflux were evaluated. Their cytotoxicity and hemolytic activity were also measured. The in vitro mechanism of the action of the new peptides were explored. Adult apolipoprotein $E^{-/-}$ mice were used to evaluate the anti-atherosclerotic activity of the best candidate, and the mechanistic basis of its anti-atherosclerotic effects were explored.

Key Results: Seventeen new AMPs (P1–P17) were synthesized and their cholesterol efflux activity and cytotoxicity were closely related to their hydrophobicity. P12 (FLEKLKELLEHLKELLTKLL), as the best candidate, most strongly promoted cholesterol

efflux among the non-toxic peptides (P1–P12). With its phospholipid affinity, P12 can effortlessly facilitate cholesterol transport through ATP-binding cassette transporter A1. In vivo, P12 exhibited prominent anti-atherosclerotic activity via coupling with HDL.

Conclusions and Implications: P12 featured proper hydrophobicity, which ensured its efficient binding with cytomembrane phospholipids, cholesterol, and HDL and provided a basis for its ability to reversely transport cholesterol and treat atherosclerosis.

Keywords: Atherosclerosis, apolipoprotein A-I mimetic peptide, hydrophobicity, lipoprotein, cholesterol

Abbreviations: ABCA1, ATP-binding cassette transporter A1; ApoA-I, apolipoprotein A-I; AMP, ApoA-I mimetic peptide; C-TPP, 5-(4-carboxyphenyl)-10, 15, 20-triphenylporphyrin; DMPC, Dimyristoyl phosphatidylcholine; RCT, reverse cholesterol transport. TC, total cholesterol; TG, triglyceride.

1. Introduction

Reverse cholesterol transport (RCT) has received increasing attention as an anti-atherosclerotic strategy in recent decades (Lewis & Rader, 2005; Ohashi, Mu, Wang, Yao & Chen, 2005). However, despite intense efforts, drugs specifically designed to stimulate RCT are barely available in the market (Reddy, Navab, Anantharamaiah & Fogelman, 2014). In vivo, HDL undergoes RCT, thereby removing parts of cholesterol from peripheral cells (Fisher, Feig, Hewing, Hazen & Smith, 2012). In the formation of HDL, lipid-free apolipoprotein A-I (apoA-I) is synthesized and secreted from the liver, after which it binds phospholipids through interactions with ATP-binding cassette transporter protein A1 (ABCA1) and forms nascent disc-shaped HDL (preβ-HDL) particles. Preβ-HDL particles constantly encapsulate peripheral intracellular cholesterol ester into its hydrophobic core to generate mature spherical HDL (α-HDL) and have stronger cholesterol carrying capacity than mature α-HDL particles. Eventually, cholesterol ester is removed from HDL and transported into hepatocytes via scavenger receptor BI (SR-BI) or transferred to LDL by cholesterol ester-transfer protein. Thus, cholesterol is mobilized and transferred from the peripheral tissues to the liver throughout the RCT process (Khera & Rader, 2010).

ApoA-I, a structural and functional protein of HDL, is the key protein that drives the RCT process. (Mei & Atkinson, 2015). ApoA-I consists of 243 amino acids and is divided into 10 amphipathic α-helical fragments by proline (Leman, Maryanoff & Ghadiri, 2014). These 10 fragments share common structural features (Ingenito et al., 2010; Islam et al., 2018): 1) Their secondary structure is an amphiphilic α-helix that continuously possesses hydrophobic and hydrophilic surfaces at proper. 2) The connection points of amphiphilic surfaces are

positively charged amino acid residues, such as Lys, Arg, and His. 3) The middle of the hydrophilic surface contains negatively charged amino acid residues, such as Asp and Glu. These characteristics are closely related to its activity. ApoA-I has high lipid affinity and drastically promotes peripheral cell cholesterol efflux. Unfortunately, the use of apoA-I as a drug has been restricted by its high production cost and lack of oral bioavailability. Fortunately, apoA-I mimetic peptides (AMPs) may represent alternative treatment options. Therefore, based on their sequence characteristics, many AMPs with short sequences have been derived. The class A and amphipathic α-helix peptide, 18A (DWLKAFYDKVAEKLKEAF) was designed to mimic apoA-I, which has hydrophobic amino acids (W, L, A, F, Y, V) on the hydrophobic face and hydrophilic amino acids (D, E, K, R) on the hydrophilic face of its α-helix, as well as a positively charged amino acid (K) at the hydrophobic/hydrophilic interface and a negatively charged amino acid (D or E) at the center of the hydrophilic face. 18A was found to associate strongly with liposomes and displace apoA-I from native HDL and apolipoprotein E (apoE) from native VLDL (Getz & Reardon, 2011). 5A (DWLKAFYDKVAEKLKEAF-P-DWAKAAYDKAAEKAKEAA), a proline-linked dimer of 18A and its derivative, more strongly promoted cholesterol efflux than 18A. This dimer readily complexed with phospholipids and formed an HDL-like structure (Amar et al., 2010). 4F (Ac-DWFKAFYDKVAEKFKEAF-NH_2), which was produced by replacing the leucine of 18A at sites 3 and 14 with phenylalanine, is the most representative AMP. L-4F (L-amino acid) and D-4F (enantiomer of L-4F) were revealed to have good cholesterol efflux activity in vitro and in vivo. In clinical research, oral and intraperitoneal 4F reduced evolving atherosclerotic lesions, plaque lipids, and macrophage activity in vein grafts, but the drug did

not affect established lesions in the aortic sinus. In addition, its dosage and cost of production were major issues in the project (Navab et al., 2002; Navab et al., 2011; Osei-Hwedieh, Amar, Sviridov & Remaley, 2011). These AMPs feature the aforementioned three common sequence-structure characteristics of the 10 fragments of apoA-I.

Regarding the anti-atherosclerotic mechanism of AMPs, after binding to HDL, the peptides promote RCT from arteriosclerotic plaques to the liver. AMPs must have a strong affinity with phospholipids and cholesterol in HDL or cells to transport cholesterol (Stoekenbroek, Stroes & Hovingh, 2015). Cholesterol efflux is a rate-limited step in the process of RCT. The factors affecting cholesterol efflux induced by AMPs are hydrophobicity, charge, and secondary structure (Leman, Maryanoff & Ghadiri, 2014). Among them, hydrophobicity is the most important and fundamental factor, that can both affect the solubility and absorption of the peptide, and directly determine its lipid affinity and secondary structure (Sviridov et al., 2013). Sufficient hydrophobicity of AMPs can promote binding between AMPs and ABCA1 for membrane phospholipid efflux to form preβ-HDL and induce cellular cholesterol efflux (D'Souza et al., 2010). In short, hydrophobicity has a considerable influence on cholesterol efflux induced by AMPs, highlighting the need for detailed studies of this variable.

Chroni and colleagues found that amino acids 220–231 of apoA-I comprise the binding domain of ABCA1 (Chroni et al., 2003). The tenth helix of apoA-I (containing amino acids 220–231) is the least conserved but most indispensable sequence (Palgunachari et al., 1996; Panagotopulos, Witting, Horace, Hui, Maiorano & Davidson, 2002). Truncation mutants of apoA-I lacking the tenth helix do not promote cholesterol efflux (Panagotopulos, Witting,

Horace, Hui, Maiorano & Davidson, 2002). In the present study, based on apoA-$I_{221–240}$, which comprises the active fragment of the apoA-I C-terminal (Wool, Reardon & Getz, 2014), 17 new AMPs were designed (P1–P17) and synthesized by gradually increasing their hydrophobicity through amino acid replacement. The relationships of hydrophobicity with the secondary structures, anti-atherosclerotic activity, and toxicity of the new mimetic peptides were evaluated. Of these, P12, a lipid-free 20-amino acid AMP featuring an amphiphilic α-helix structure and the best biological function of apoA-I, was revealed to have the greatest effects on cholesterol efflux. The anti-atherosclerotic mechanisms and effect of the candidate AMP were elucidated in $apoE^{-/-}$ mice.

2. Methods

2.1 Peptide and fluorescent probe synthesis

ApoA-$I_{221–240}$, 17 novel AMPs (P1–P17), L-4F, and 5-(4-carboxyphenyl)-10, 15, 20-triphenylporphyrin (C-TPP)-labeled P12 were synthesized using Wang resin and N-9-fluorenyl methoxycarbonyl (Fmoc) based on solid-phase peptide synthesis. The peptide extension reaction conditions were as follows: 3-fold excess of 2-(1H-benzotriazol-1-yl)-1, 1, 3, 3-tetramethyluronium hexafluorophosphate (HBTU)/hydroxybenzotriazole (HOBt) as the coupling reagents, N-dimethylformamide as a solvent, 6-fold excess of diisopropylethylamine, and 3-fold excess of Fmoc protecting group amino acids. The cleavage of the peptide from the resin was performed using a reagent composed of 95% trifluoroacetic acid, 2.5% triisopropylsilane, and 2.5% deionized water (3 h, room temperature). The peptide was precipitated in diethyl ether (1:1, volume ratio).

C-TPP and C-TPP-P12 were generated as described previously (Ushasri et al., 2014). Briefly, 4-carboxybenzaldehyde and benzaldehyde were mixed with propionic acid. The reaction mixture was heated up to 120°C, and pyrrole was added dropwise. The obtained solid material was subjected to silica gel column chromatography and eluted with CH_2Cl_2/CH_3OH to obtain pure C-TPP. Then 1 equivalent of P12 that was not cleaved from the resin, 10 equivalents of C-TPP, 10 equivalents of HBTU and 10, equivalents of HOBt were dissolved in dimethylformamide separately and mixed. This mixture was added to the resin, and 10 equivalents of diisopropylethylamine were added to start the coupling reaction. After 24 h, the resin was dried, and the cleavage of peptide from the resin was achieved by treatment using a solution containing trifluoroacetic acid at room temperature for 10 h (Figure S1 and S2).

The obtained crude peptides were purified by reversed-phase-HPLC (Waters, MA, USA) on a C_{18} column (19 mm × 250 mm). The hydrophobicity and purity of the peptides were analyzed using reversed-phase-HPLC on a C_{18} column (4.6 mm × 250 mm). All peptides prepared were more than 95% pure. Their molecular masses were confirmed via electrospray ionization MS (MaXis 4G, Bruker, USA).

2.2 The design strategy of AMP

As shown in Table 1 and Figure 1, 17 novel AMPs were designed and synthesized using apoA-$I_{221–240}$ (VLESFKVSFLSALEEYTKKL) as the parent peptide. To ensure alignment to the amphiphilic surface of apoA-$I_{221–240}$, L_2, S_4, F_5, V_7, S_8, F_9, L_{10}, S_{11}, L_{13}, E_{15}, Y_{16}, and K_{19} of apoA-$I_{221–240}$ were replaced with V_2, K_4, A_5, E_7, A_8, A_9, E_{10}, H_{11}, K_{13}, A_{15}, A_{16}, and A_{19}, respectively. Then, the amino acids on the hydrophilic surface of the new peptides were

confirmed, The template of the novel AMPs was $X_1X_2EKX_5KEX_8X_9EHX_{12}KEX_{15}X_{16}TKX_{19}X_{20}$ (X represents hydrophobic amino acids), and the hydrophobicity of P1–P17 was gradually increased by replacing the hydrophobic amino acid with Ala, Leu, Val, Phe or Trp. Hydrophobicity and the hydrophobic moment were calculated using HeliQuest online software.

2.3 Circular dichroism (CD) measurements

To study the relationship between the secondary structures and cholesterol efflux activity of the new peptides, the CD spectra of the peptides were measured at 25°C on a J-810 spectrometer (Jasco, Japan) using a quartz cell with a 1.0 mm path length. Recording was performed over the range of 190–260 nm with a scanning speed of 50 $nm \cdot min^{-1}$, band width of 1 nm, and response time of 1 s. The peptide solutions were prepared at a final concentration of 50 μM in deionized water (mimicking an aqueous environment) and 50% trifluoroethanol (TFE, mimicking the hydrophobic environment of the biological membrane). The acquired CD spectra were then converted to the mean residue ellipticity using the following equation:

$$\theta_M = (\theta_{obs} \times 1000)/(c \times l \times n),$$

where θ_M is the residue ellipticity ($deg \cdot cm^2 \cdot dmol^{-1}$), θ_{obs} is the observed ellipticity corrected for the buffer at a given wavelength (mdeg), c is the peptide concentration (mM), l is the path length (mm), and n is the number of amino acids.

2.4 DMPC vesicle solubilization assay

Dimyristoyl phosphatidylcholine (DMPC) vesicles (1 $mg \cdot mL^{-1}$) were prepared by resuspending DMPC in 75°C PBS (pH= 7.4) and vortexed. Then, 5 μL of 1mM AMP in PBS

(pH= 7.4) was added to 96-well plates, followed by 95 μL of 1 $mg \cdot mL^{-1}$ DMPC vesicles in PBS. The working concentration of the peptide was 50 μM. Changes in light scattering upon peptide addition were monitored at 23.9°C every 15 s for 90 min at 430 nm, with shaking in a multimode plate reader. Each sample had five parallel duplicates and the test was repeated in five to six independent experiments.

2.5 Cell culture

RAW264.7 cells (RRID:CVCL_0493) were cultured in DMEM supplemented with 10% FBS, and THP-1 cells (RRID:CVCL_0006) were cultured in RPMI-1640 medium supplemented with 10% FBS. Cells were maintained at 37°C in 5% CO_2.

2.6 Determination of cellular cholesterol efflux

The cholesterol efflux activity of the new peptides was determined using a previously described method with modifications (Avdulov, Chochina, Igbavboa & Wood, 2000; Zhang et al., 2017). Briefly, RAW264.7 cells ($4 \times 10^4 \cdot well^{-1}$) or THP-1 ($1 \times 10^4 \cdot well^{-1)}$ were labeled with 22-NBD-cholesterol ($2.5\ mg \cdot L^{-1}$) for 24 h in serum-free medium, and then cellular cholesterol efflux was examined in the presence of 0, 1, 2, 5, 10, 20, 50, 100 or 200 μM AMPs for 12 h in serum-free medium. Cells were lysed with 2% Triton X-100. The fluorescence intensity (FI, Ex = 469 nm, Em = 538 nm) of 22-NBD-cholesterol in medium and cell lysates was monitored using a multimode reader. The cholesterol efflux rate was calculated as $(FI_{medium})/(FI_{medium} + FI_{cell}) \times 100\%$. Each sample had five parallel duplicates, and the test was repeated in five to six independent experiments.

For the further determination of cholesterol efflux using flow cytometry, RAW264.7 and THP-1 cells were labeled with 22-NBD-cholesterol ($2.5\ mg \cdot L^{-1}$) for 24 h in 24-well plates,

and cellular cholesterol efflux was induced by incubation with apoA-$I_{221–240}$ (10 μM), L-4F (10 μM), or P12 (1, 10 and 20 μM) for 12 h. The uptake and efflux of 22-NBD-cholesterol (Ex = 488 nm, Em = 550 nm) in cells were determined using a flow cytometer (LSRFortessa, BD). Each sample had five parallel duplicates, and the test was repeated in five to six independent experiments.

Finally, ABCA1-dependent cellular cholesterol efflux stimulated by P12 was determined using two methods:

In the first method (Shimizu et al., 2015; Uehara et al., 2013), RAW264.7 or THP-1 cells were labeled with 22-NBD-cholesterol (2.5 $mg \cdot L^{-1}$) for 12 h in serum-free medium. Cells were washed with PBS (pH= 7.4). To promote the ABCA1 expression, the labeled cells were treated with 9-cis-retinoic acid (retinoid X receptor ligand) and TO-901317 (liver X receptor agonist) for 10 h in serum-free medium (each 5 μM). To suppress ABCA1 function, cells were treated with 20 μM probucol for 2 h at 37°C. Intracellular cholesterol efflux was induced by treatment with P12 (1 and 10 μM) for 4 h, and L-4F was used as a positive control. FI of 22-NBD-cholesterol in medium and cell lysates was monitored using a multimode reader.

In the second method (Carballo-Jane et al., 2010), RAW264.7 or THP-1 cells were labeled with 22-NBD-cholesterol (2.5 $mg \cdot L^{-1}$) for 24 h in serum-free medium, and then cellular cholesterol efflux was induced by exposure to P12 (0, 1, 5, 10 and 20 μM) while providing energy for ABCA1 activity using cAMP (0.3 mM) for 12 h in serum-free medium. L-4F was used as a positive control. FI of 22-NBD-cholesterol in medium and cell lysates was monitored using a multimode reader.

2.7 Cytotoxicity assay and hemolytic activity

RAW264.7 cells were seeded on 96-well plates at a density of 1×10^4 • $well^{-1}$. After permitting adherence for 6 h, 100 μL of AMP (0, 1, 2, 5, 10, 20, 50, 100, or 200 μM) in serum-free medium was added to the plates for 12 h, after which 10 μL of MTT (50 $mg\cdot mL^{-1}$ in waters) was added. After 4 h, the formazan in the cells was dissolved in DMSO. The absorbance was measured using a multimode reader at 490 nm. Each sample had five parallel duplicates, and the test was repeated in five to six independent experiments.

The venous blood of C57BL/6J mice (male, 20 ± 2 g) was collected from the venous plexus of the fundus and centrifuged at 1000 × g for 10 min. The plasma supernatant was removed, and 8% erythrocyte suspension was prepared with PBS (pH= 7.4). Then, 100 μL of 8% erythrocyte suspension and 100 μL of AMPs (0, 1, 2, 5, 10, 20, 50, 100, or 200 μM) in PBS were added to the 96-well plates, and 2% Triton X-100 was used as a positive control. The plates were incubated at 37°C for 1 h and then centrifuged at 12,000 × g for 15 min. Plasma supernatants (150 μL) were transferred to new 96-well plates. The absorbance was measured using a multimode reader at 490 nm. Each sample had five parallel duplicates, and the test was repeated in five to six independent experiments.

2.8 Localization of P12 and 22-NBD-cholesterol in macrophages

As described previously, THP-1 and RAW264.7 were labeled with 22-NBD-cholesterol (2.5 $mg\cdot L^{-1}$) for 24 h in laser-scanning confocal microscope (LSCM) dishes, and cellular cholesterol efflux was induced by exposure to C-TPP-P12 for 12 h. The fluorescent images of cells were photographed in track 1 (22-NBD-cholesterol, Ex = 488 nm, Em = 500–550 nm, green), track 2 (C-TPP-P12, Ex = 515 nm, Em = 640–730 nm, red), and the bright-field via

LSCM (LSM710, Zeiss).

2.9 Animal experiments

2.9.1 Animal management

All experiments involving animals were performed according to protocols approved by the Animal Care and Use Committee of Lanzhou University. Mice were purchased from Beijing Charles River Laboratories, maintained in a temperature- and light-controlled facility, and fed specific pathogen-free chow. ApoE$^{-/-}$ mice and background wild-type C57BL/6J mice (RRID:IMSR_JAX:000664) 20 ± 1 g, 10 weeks were used for the in vivo experiments. Background wild-type C57BL/6J mice (n=10, 5 females and 5 males) were fed a commercial basal diet and apoE$^{-/-}$ mice (n = 60, 30 females and 30 males) were fed a high-fat diet (0.5% cholesterol and 10% fat). After 4 weeks, apoE$^{-/-}$ mice were divided into six groups. Low and high doses (10 and 20 mg·kg^{-1}, respectively) of P12 were injected intraperitoneally into mice three times per week for 12 weeks. Saline, L-4F (10 mg·kg^{-1}), and apoA-I$_{221–240}$ (10 mg·kg^{-1}) were used as background, positive, and negative controls, respectively. After 16 weeks, mice were anesthetized with isoflurane and killed via cervical dislocation, after an overnight fast. Plasma samples, organs, and tissues were then collected.

Other batches of wild-type C57BL/6J (n=20, male) and apoE$^{-/-}$ (n = 20, male) mice were fed using the aforementioned method for the following four supplementary experiments: the determination of plasma apoA-I levels after P12 injection, plasma clearance of P12, the effects of 1 week of P12 exposure on blood lipid levels, and the effect of 2 weeks of P12 on cholesterol excretion (five C57BL/6J and five apoE$^{-/-}$ mice for each experiment).

In all experiments, animals were randomly assigned to treatment groups. The numbers of mice in each group are designated in the individual figures. The sample size in each group was determined according to previous studies with similar experimental protocols. The studies were blinded for treatment assignment and outcome assessment. Animal studies are reported in compliance with the ARRIVE guidelines (Kilkenny, Browne, Cuthill, Emerson & Altman, 2010) and with the recommendations made by the *British Journal of Pharmacology*.

2.9.2 Histopathological examination

Paraffinized sections of the aortic arch were stained with hematoxylin and eosin. The images were captured using a CX21 microscope (Olympus, Japan). The atherosclerotic lipid plaque and relative thickness of the arterial wall were quantified via computer image analysis using Adobe Photoshop CC 2017 software (RRID: SCR_014199).

2.9.3 Serum lipid profiles, turbidity, inflammatory factors, and lipid peroxidation

Serum levels of total cholesterol (TC), LDL-C, HDL-C, triglyceride (TG), and C-reactive protein (CRP) were determined using biochemical kits according to the manufacturer's instructions on an automatic biochemical analyzer (Hitachi, Japan). Serum IL–6, monocyte chemoattractant protein-1 (MCP-1), and TNF-α levels were measured using ELISA assay kits according to the manufacturer's protocol. Serum turbidity was represented as the absorbance as measured using a multimode reader at 430 nm. Serum malondialdehyde (MDA) and superoxide dismutase (SOD) levels were determined in all mice using biochemical kits according to the manufacturer's instructions.

2.9.4 Plasma clearance of P12 in C57BL/6J and apoE$^{-/-}$ mice

Both wild-type C57BL/6J (n = 5) and apoE$^{-/-}$ mice (n = 5) were intravenously administered 10 mg·kg^{-1} P12. P12 levels in plasma were measured using HPLC at 0, 1, 5, 10, 15, 30, 60, 90, 120, 180, 240, 360, 480, 720, 1440, and 2880 min after injection. The half-life ($t_{1/2}$) of P12 in plasm were calculated in C57BL/6J and apoE$^{-/-}$ mice using Microsoft Excel 2019 (Microsoft Excel, RRID: SCR_016137).

2.9.5 Effect of P12 on plasma apoA-I levels

Plasma apoA-I levels in wild-type C57BL/6J (n=5) and apoE$^{-/-}$ mice (n=5) were measured before and after the intravenous injection of P12 (10 mg·kg^{-1}) using an apoA-I assay kit.

2.9.6 Regulative effect of 1 week of P12 exposure on blood lipids

Five new male apoE$^{-/-}$ mice were maintained on their diets for 1 week after 4 months of feeding with the high-fat diets. Five new male wild-type C57BL/6J mice were used as the control group. They received intraperitoneal injections of P12 (10 mg·kg^{-1}·day^{-1}). Serum TC, LDL-C, HDL-C, and non-HDL-C levels were measured in both mouse groups before and after daily P12 administration.

2.9.7 Effect of P12 on cholesterol excretion for two weeks

After 4 months of feeding, an additional five male apoE$^{-/-}$ mice fed with aforementioned high-fat diets and five male wild-type C57BL/6J mice fed with basal diets were maintained on their respective diets for 2 additional weeks. In the first week, feces were collected from mice in each group. In the second week, mice received intraperitoneal injections of P12 (10 mg·kg^{-1}·day^{-1}). Feces were collected for measuring of cholesterol levels. To extract the

cholesterol, 1 g of feces powder was soaked in 5 mL of chloroform and shaken 10 min on a vortex mixer. After filtering samples, non-cholesterol impurities in chloroform were extracted using water, and cholesterol in chloroform was measured using a cholesterol kit according to the manufacturer's instructions.

2.10 In vivo mechanism experiments

2.10.1 Lipoprotein analysis by size exclusion chromatography

Fresh blood was drawn from apoE$^{-/-}$ mice into tubes containing potassium EDTA, and plasma was separated immediately by centrifugation at 500 × g for 30 min at 4°C. In total, 5 μL of peptides (P12 and C-TPP-P12, final concentration = 0.25 mg·mL^{-1}) were mixed with 45 μL of mouse plasma and incubated at 37°C for 2 h. Size exclusion chromatography was performed at ambient temperature using a Superose 6 column (10 × 1000 mm) on a semi-preparative HPLC system (Waters). A 200 μL aliquot of the peptide/plasma mixture was injected per run and eluted in PBS (pH= 7.4) with 1 mM EDTA at a flow rate of 1 mL·min^{-1}. A total of 60 fractions (1.5 mL·fraction^{-1}) were directly collected into microtiter plates for further analysis. The TC content in each fraction was measured using a cholesterol kit according to the manufacturer's instructions and FI represented the C-TPP-P12 concentration in each fraction. Saline was used as a control.

2.10.2 Western blot quantification of mouse preβ-HDL levels

The western blotting procedures and analysis were performed according to the *BJP* guidelines (Alexander et al., 2018). Peptide solution (5 μL) was mixed with 45 μL of apoE$^{-/-}$ mouse plasma, incubated at 37°C with shaking at 300 rpm for 2 h, and then subjected to one-dimensional, non-reducing, anti-mouse apoA-I Western blotting. Briefly, samples were

diluted 1:1 with Tris-glycine native sample buffer, and 4–20% native polyacrylamide gel electrophoresis as performed at 90 V for 10 min and at 150 V for 1 h. Proteins were transferred to a PVDF membrane (0.45 μm) overnight (200 mA at 4°C). After transfer, the membrane was blocked with 6% lipid-free milk and washed three times with Tris-buffered saline with Tween-20 (10 mM Tris, pH 7.4, 150 mM NaCl, and 0.1% Tween-20). Rabbit anti-mouse apoA-I antibody (1:500) and HRP-conjugated goat anti-rabbit antibody (1:1000) were used as the primary and secondary antibodies, respectively. Blots were developed using the HRP substrate luminol reagent and scanned using a Typhoon 9400 Imager (GE Healthcare, Piscataway, NJ, USA). Preβ-HDL was identified on the basis of its electrophoretic mobility, and the band was quantified using Adobe Photoshop CC 2017 software (Adobe Photoshop, RRID:SCR_014199). The results were expressed as the gray value representing the signal intensity of the band.

2.11 Data and analysis

The data and statistical analysis comply with the recommendations of the *British Journal of Pharmacology* on experimental design and analysis in pharmacology (Curtis et al., 2018). All experiments were randomized and blinded. The sample size in each group was determined based on our previous studies with similar experimental protocols. At least five samples per group (n = 5) were included in the statistical analysis, where n is the number of independent values. Date for animals in which relative arterial wall thickness could not be measured because of the rupture of arterial plaque were excluded from the analysis. A normal probability plot was used to examine data distributions. Statistical analyses were performed using GraphPad Prism 5 software (GraphPad Prism, RRID: SCR_002798), and data are

presented as mean ± SEM unless otherwise stated. Student's *t*-test was used for comparisons between two groups. For comparisons of three or more groups, one-way ANOVA followed by Dunnett's *post-hoc* test was used for normal distributions with one variable. The significance level was set at $P < .05$.

2.12 Materials

22-NBD-cholesterol, DMEM, RPMI-1640, and FBS were purchased from Thermo Fisher Scientific (MA, USA). Serum TC, LDL-C, HDL-C, TG, and CRP assay kits were purchased from Maccura Biotechnology Co., Ltd. (Sichuan, China). IL-6, MCP-1, and TNF-α assay kits were purchased from Cloud-Clone Corp (Beijing, China). 9-cis-retinoic acid, TO-901317, cAMP, MDA, and SOD were purchased from Sigma-Aldrich (St. Louis, MO, USA). A cholesterol assay kit was purchased from Beijing Apllygen Gene Technology Co. LTD (Beijing, China). Rabbit anti-mouse apoA-I antibody (Proteintech Cat# 14427-1-AP, RRID: AB_2056524) and HRP-conjugated goat anti-rabbit antibody (Proteintech Cat# SA00001-2, RRID: AB_2722564) were purchased from Proteintech Group, inc. (IL, USA).

2.13 Nomenclature of targets and ligands

Key protein targets and ligands in this article are hyperlinked to corresponding entries at http://www.guidetopharmacology.org (IUPHAR/BPS Guide to Pharmacology, RRID:SCR_013077), the common portal for data from the IUPHAR/BPS Guide to Pharmacology (Harding et al., 2018), and are permanently archived in the Concise Guide to Pharmacology 2017/18 (Alexander, Christopoulos et al., 2017; Alexander, S. P. H., Fabbro et al., 2017; Alexander, Peters et al., 2017).

3. Results

3.1 Secondary structure and retention time was influenced by hydrophobicity

Changes in the secondary structures of the new AMPs were observed with the increases in hydrophobicity. In aqueous medium, apoA-$I_{221–240}$ and P1–P10 did not form α-helices, whereas L-4F and P11–P14 had stable α-helical conformations. Interestingly, P15–P17 had β-sheets conformations. In the simulated cell membrane environment of 50% TFE, apoA-$I_{221–240}$, L-4F, and P1–P14 had α-helical structures, whereas P15–P17 had α-helical and β-sheet structures (Figure 2a, 2b, and S3).

The hydrophobicity and hydrophobic moment of P1–P17 had a linear relationship (Figure 2c). The retention time (t_R) of these new peptides were measured using the analytical HPLC. The result illustrated that t_R of P1–P12 gradually increased, whereas those of P12–P17 gradually decreased. However, the theoretical value of hydrophobicity was increased from P1 to P17 (Figure 2d).

3.2 The lipid affinity of P12 ensures its cholesterol efflux activity

Macroscopically, the DMPC emulsion is dissolved by sufficiently hydrophobic AMPs into a clear liquid. Of the studied AMPs, apoA-$I_{221–240}$ and P1–P8 induced no changes of the DMPC emulsion within 90 min. However, P9–P11, and L-4F quickly dissolved in DMPC within 10 min. Meanwhile, the emulsion became gradually clear in the presence of P12–P17, but the emulsion became completely clear after 90 min only following exposure to P12 (Figure 2e).

3.3 P12, a new peptide with excellent activity and low toxicity, was identified

In RAW264.7 cells, apoA-$I_{221–240}$ and P1–P5 did not induce cholesterol efflux, and their intracellular cholesterol efflux rates were less than 2% at concentrations of 1–200 μM. L-4F and P6–P17 displayed concentration-dependent cholesterol efflux activity. When the concentration exceeds the safe limit, P13–P17 could damage the membrane of RAW264.7 cells, leading to cholesterol leakage from cells and consequent changes of the dose-effect curves (Table 2, Figure 3a, S4, and S5).

Then, the cytotoxicity of these new mimetic peptides were determined in RAW264.7 cells. The results illustrated that apoA-$I_{221–240}$ and P1–P12 had no cytotoxic effects. P13 had significant cytotoxicity at concentrations of 100 and 200 μM, resulting in cell viability rates of less than 80%. P14 and P15 exhibited cytotoxic effects at 20 and 5 μM, respectively. P16, P17, and L-4F had concentration-dependent cytotoxic effects in RAW264.7 cells (Table 2, Figure 3b).

The influence of new mimetic peptides on mouse erythrocytes in comparison with their parent peptide and L-4F is presented in Table 2 and Figure S6. After 12 h, apoA-$I_{221–240}$, P1–P13, and L-4F induced slight hemolysis, and the hemolytic rate was less than 2% at a concentration of less than 200 μM. P14 was hemolytic at concentrations exceeding 200 μM (hemolytic rate >2%). P15–P17 induced obvious hemolysis at 20 μM, and the hemolytic rate approached 8% at 200 μM. Based on these results, P12, with good activity and no toxicity, was screened for further study.

3.4 In vitro mechanism

3.4.1 P12 can promote cholesterol efflux in macrophages

P12 more strongly induced cholesterol efflux in THP-1 cells than in RAW264.7 cells (Figure 4a).

The results of cholesterol efflux determination using flow cytometry are shown in Figure 4b. Compared with the findings in of PP (apoA-$I_{221–240}$), both P12 and L-4F significantly promoted the intracellular cholesterol efflux at 10 μM in both RAW264.7 (efflux rates of 3.2 and 4.56%, respectively) and THP-1 cells (efflux rates of 5.5 and 9.89%, respectively). ApoA-$I_{221–240}$ did not display distinctive cholesterol efflux activity in either cell line (efflux rates of 0.18 and 0.59%, respectively, at 10 μM).

3.4.2 P12 induced cholesterol efflux through ABCA1

P12 promotes cholesterol efflux through ABCA1. After treatment with 9-cis-retinoic acid and TO-901317, P12 increased cholesterol efflux in RAW264.7 cells by 0.40% at 1 μM and 1.02% at 10 μM. Meanwhile, and Probucol suppressed the cholesterol efflux induced by P12. Similar results were obtained for L-4F. ABCA1-dependent cellular cholesterol efflux was more strongly induced by 9-cis-retinoic acid and TO-901317 in THP-1 cells than in RAW264.7 cells. P12 increased cholesterol efflux by 1.53% at 1 μM and 1.92% at 10 μM in THP-1 cells. Meanwhile, in the presence of Probucol, P12-induced cellular cholesterol efflux was reduced by 1.75% at 1 μM and 2.18% at 10 μM (Figure 4c).

In both RAW264.7 and THP-1 cells, P12-induced cholesterol efflux was obviously enhanced by treatment with cAMP. Unexpectedly, L-4F was cytotoxic in THP-1 cells, leading to cholesterol release at concentrations exceeding 10 μM (Figure 4d). It is shows that P12 has

stronger ABCA1-dependent cholesterol efflux activity than L-4F.

3.4.3 P12 promoted cholesterol efflux by acting on the cell membrane

To further confirm the acting site of P12, the fluorescence of 22-NBD-cholesterol and P12 labeled with C-TPP were examined in RAW264.7 and THP-1 cells. As shown in Figure 4e, 22-NBD-cholesterol had a strong fluorescent signal throughout RAW264.7 and THP-1 cells excluding the nucleus at 24 h, but C-TPP-P12 fluorescence was only observed outside the cell or on the cell membrane. Moreover, THP-1 cells exhibited much greater membrane fluorescence for C-TPP-P12 than RAW264.7 cells. This result was consistent with the results in Figure 4a and b.

3.5 Animal experiment

3.5.1 P12 suppressed the abnormal thickening of the arterial wall

The typical pathological characteristics of atherosclerosis were confirmed in apoE$^{-/-}$ mice (Figure S9). The therapeutic effect of P12 is presented in Figure 5a and b. The statistical analysis illustrated that the relative intimal thickening and plaque size of each sample were significantly decreased by P12. The relative thickness of the arterial wall in male apoE$^{-/-}$ mice was reduced by L-4F, their parent peptide, and low- and high-doses of P12 by 80.24, 45.48, 90.26, and 94.46%, respectively, and by 69.64, 39.50, 84.88, and 92.04%, respectively, in female apoE$^{-/-}$ mice.

3.5.2 P12 has lipid-lowering, anti-inflammatory and anti-oxidative effects in apoE$^{-/-}$ mice

Serum turbidity and MDA, TG, TC, HDL-C, and LDL-C levels were significantly higher in apoE$^{-/-}$ mice than in wild-type mice after 4 months of feeding. P12 significantly prevented

lipid accumulation and peroxidation in blood vessels. SOD levels were increased by P12 in apoE$^{-/-}$ mice. Serum HDL-C levels were higher in un-treatment apoE$^{-/-}$ mice than in wild-type mice after 4 months. HDL-C levels were increased by high doses of P12 in apoE$^{-/-}$ mice ($P < .05$). TC, TG, and LDL-C levels were dramatically reduced by P12 in apoE$^{-/-}$ mice ($P < .05$). After 4 months of feeding. the gender differences in serum lipids (TG, TC, HDL-C, and LDL-C) were obvious. Serum lipids levels were lower in female mice than in male mice. Serum TG and TC levels were more strongly lowered by P12 in male mice than in female mice. P12 had no significant effect on serum HDL-C levels in female or male mice, whereas it reduced LDL-C levels in female and male mice by the same extent (Figure 5b and c).

After high-fat diet feeding, serum CRP, IL-6, MCP-1, and TNF-α levels were significantly higher in apoE$^{-/-}$ mice than wild-type mice ($P < .05$). Meanwhile, P12 significantly suppressed these inflammatory indices. The apoA-I$_{221–240}$ had no cholesterol efflux activity in vitro and no satisfactory lipid-lowering activity in vivo, although it exhibited favorable anti-inflammatory effects. CRP levels were close to 0 mg·L^{-1} in wild-type mice compared with more than 150 mg·L^{-1} in apoE$^{-/-}$ mice. Serum CRP levels in apoE$^{-/-}$ mice were reduced by approximately 70% by P12 treatment compared with those in un-treatment apoE$^{-/-}$ mice. After 4 months of feeding. the gender differences in serum inflammatory factor levels were extremely obvious. Excluding CRP, serum inflammatory factor levels (IL-6, MCP-1, and TNF-α) were lower in all of male mice than in all of female mice (Figure 5d).

3.5.3 P12 has a short half-life in wild-type C57BL/6J and apoE$^{-/-}$ mice

The plasma clearance curve and fitted half-life of P12 are presented in Figure 6a. No significant difference was observed in the plasma clearance rate of P12 between apoE$^{-/-}$ and C57BL/6J mice ($P = 0.9404$, t-test). However, the $t_{1/2}$ of P12 was longer in apoE$^{-/-}$ mice

(3.09 h) than in C57BL/6J mice (2.40 h). After intravenous injection, P12 remained in the plasma approximately 25 h.

3.5.4 P12 can slowly increase plasma apoA-I levels in apoE$^{-/-}$ mice within 24 h

As shown in Figure 6b, plasma apoA-I were lower in apoE$^{-/-}$ mice than in C57BL/6J mice. P12 had no effect on plasma apoA-I in C57BL/6J mice. After the intravenous injection of P12, plasma apoA-I in apoE$^{-/-}$ mice displayed a downward trend from 0 to 2.5 h and an upward trend from 2.5 to 24 h. However, after the intravenous injection of P12 for 24 h, plasma apoA-I levels were increased in apoE$^{-/-}$ mice by 0.094 g·L^{-1}.

3.5.5 P12 decreased blood lipid levels and increased cholesterol excretion on apoE$^{-/-}$ mice

P12 had indistinctive effects on serum lipids levels in wild-type C57BL/6J mice and HDL-C levels in apoE$^{-/-}$ mice after 7 days of treatment, whereas the AMP significantly reduced serum TC, LDL-C, and non-HDL-C levels in apoE$^{-/-}$ mice (Figure 6c). Similarly, P12 had no effect on cholesterol excretion in wild-type mice within 7 days whereas its treatment increased the cholesterol excretion in apoE$^{-/-}$ mice by 76.8% (Figure 6d).

3.6 P12 can bind to plasma HDL, and transform α-HDL into preβ-HDL

The results in Figure 7 illustrated that the peak HDL area was smaller in plasma treated with P12 than in plasma incubated with saline. The peak HDL area was significantly increased by incubation with C-TPP-P12 and plasma. The increased peak fluctuation of the red line was the absorbance of C-TPP-P12 (Figure 7a). As shown in Figure 7b, most of the cholesterol in saline-treated plasma was concentrated in HDL, whereas the cholesterol content of HDL was significantly reduced in P12-treated plasma. As shown in Figure 7b and c, P12 reduced TC content. C-TPP-P12 was concentrated in the peak period of HDL, which

fully indicated that C-TPP-P12 can bind to mature α-HDL.

As shown in Figure 7d and e, P12 converted α-HDL to preβ-HDL, and the conversion rates increased with increasing P12 concentrations. The preβ-HDL conversion rates in the presence of 125, 250, 500, and 1000 $\mu g \cdot mL^{-1}$ of P12 were 8.42, 17.48, 38.16, and 40.57%, respectively. Conversely, the preβ-HDL conversion rate in the presence of 500 $\mu g \cdot mL^{-1}$ L-4F was 35.12%. Interestingly, the parent peptide apoA-$I_{221–240}$ was also linked to a high preβ-HDL conversion rate at 500 $\mu g \cdot mL^{-1}$ (12.36%).

4. Discussion

This study was aimed to design new short apoA-I mimetics possessing the biological functions of apoA-I. Considering that AMPs exert anti-atherosclerotic effects through RCT, the effect of hydrophobicity on their lipid affinity and ability to transport cholesterol is a primary factor of consideration (Datta et al., 2001; Van Lenten et al., 2009). In this study, fragment 221–240 of apoA-I were used as the parent peptide because it has an essential sequence for cholesterol efflux and contains the ABCA1 binding domain (Chroni, Koukos, Duka & Zannis, 2007). In order to maintain the original sequence of apoA-$I_{221–240}$ as much as possible, the novel AMPs were designed using a strict amphiphilic construct. The hydrophobic surface is beneficial for affinity with the fatty chain of phospholipids. The positively charged amino acids at the amphiphilic junction facilitate them binding to the negatively charged phospholipid head, and the negatively charged amino acids in the middle of the hydrophilic surface can balance the positive charge and stabilize ABCA1.

This study found that new AMPs induced cholesterol efflux when the hydrophobic value was ≥ 0.260 (calculated using HeliQuest), whereas their cytotoxicity was observed at values

of ≥ 0.548. Furthermore, when their hydrophobic value was ≥ 0.699, AMPs induced slight hemolysis at high concentration. According to the in vitro mechanism studies, the possible explanations of the aforementioned results are as follows. 1) Hydrophobicity affects the secondary structure of new AMPs. As hydrophobicity increased, the secondary structure of new AMPs changed from disordered structure (P1–P10) to an α-helical (P11–P14) or β-sheet (P15–P17) structure. In line with this finding, prior research uncovered that AMPs must have an amphipathic α-helical structure to induce cholesterol efflux (Beaufils et al., 2007). In this study, P11–P14 always maintained a stable α-helical structure whether in an aqueous or the simulated biofilm environment, leading to their stronger activity and weaker cytotoxicity compared with the other AMPs. 2) Hydrophobicity affects lipid affinity and amphipathicity (represented by the hydrophobic moment) of AMPs. With an increasing hydrophobicity, AMPs exhibit increasing ability to dispersion DMPC vesicles. The result indicated that P9–P11 had good lipid affinity and appropriate amphipathicity (in line with prior findings that the moment balance between hydrophobic and hydrophilic face is important for lipid interactions) (Natarajan, Forte, Chu, Phillips, Oram & Bielicki, 2004), thereby explaining their ability to rapidly bind to micron-DMPC vesicles in water and then disperse them into nanovesicles. Although lipid affinity is the basis of their cholesterol efflux activity, P12 more strongly induced cholesterol efflux than P9–P11 despite its weaker lipid affinity. This finding also suggested that other factors, such as ABCA1 dependence, affect the cholesterol efflux activity of AMPs in addition to lipid affinity and amphipathicity (Yao, Gordon, Barochia, Remaley & Levine, 2016).

Several studies reported that apoA-I can promote the dephosphorylation of the PEST sequence of ABCA1, reduce the calpain-mediated degradation of ABCA1 and allow permit greater ABCA1 expression on the cell membrane surface, leading to the enhancement of cholesterol efflux from cells (Arakawa, Hayashi, Remaley, Brewer, Yamauchi & Yokoyama, 2004; Martinez, Agerholm–Larsen, Wang, Chen & Tall, 2003). ApoA-I promotes cholesterol efflux by binding to ABCA1 rather than impairing cell membranes. ABCA1 overexpression can enhance the cellular binding of apoA-I (Jin et al., 2016; Xie, Zhao & Li, 2010). The process of cholesterol efflux through ABCA1 is mild, and it does not impair cell membranes, leading to a smooth dose-effect curve. Similarly, our results indicated that P12 had a nearly smooth dose-effect curve and functioned together with ABCA1. LSCM also confirmed that P12 acted only on the cytomembrane surface without impairing cellular integrity.

Numerous studies have confirmed that the function of HDL is more important to anti-atherosclerotic effects than its quantity (Chapman, Orsoni, Robillard, Therond & Giral, 2018; Tsompanidi, Brinkmeier, Fotiadou, Giakoumi & Kypreos, 2010). In this study, P12 observably regressed atherosclerotic plaques in apoE$^{-/-}$ mice, although serum HDL-C levels did not fluctuate after the 12 weeks of P12 treatment. A possible mechanism for P12-induced plaque suppression might be the promotion of HDL function. Moreover, P12 can slowly increase the concentration of apoA-I within 24 h. These findings illustrate that P12 can increase the ability of HDL to block the accumulation of harmful lipids in the body. Unexpectedly, the hypolipidemic effect of P12 was better at 10 mg·kg^{-1} than at 20 mg·kg^{-1} of P12, suggesting that excessive P12 affected some functions of HDL. In addition to RCT, HDL also prevents atherosclerosis through anti-inflammatory effects. Interestingly, apoA-

$I_{221–240}$ had excellent anti-inflammatory effects in atherosclerotic mice, suggesting that P12 retained the anti-inflammatory properties of its parent peptide. The findings indicate that P12 can potentially treat atherosclerosis by lowering blood lipid levels, promoting cholesterol excretion, suppressing inflammation, and reducing lipid peroxidation. In addition, gender differences lead to differences in blood lipids, lipid peroxidation and inflammatory factors were observed.

As mentioned previously, HDL consists of nascent HDL particles (pre β-HDL, size approximately 7.2 nm) and mature HDL particles (α-HDL, size approximately 12.2 nm) according to its electrophoretic mobility (Tsompanidi, Brinkmeier, Fotiadou, Giakoumi & Kypreos, 2010). Compared with α-HDL, preβ-HDL is a cholesterol-unsaturated moiety containing less cholesterol and cholesterol ester content. When preβ-HDL loads cholesterol to saturation, it becomes α-HDL. Thus, preβ-HDL has a stronger ability to carry and load cholesterol than α-HDL, making it a key molecule for the HDL function (Hafiane & Genest, 2015). Our results illustrated that P12 promoted the function of HDL remodeling α-HDL into preβ-HDL. Further analysis indicated that P12 can bind with the phospholipids of HDL to promote RCT, thereby improving its efficiency.

Overall, as a novel developed AMP with an amphipathic α-helical structure, P12 has stronger ABCA1-dependent cholesterol efflux activity and lower cytotoxicity than L-4F, and it can significantly suppress the formation of atherosclerotic plaque by promoting the cholesterol efflux from the plaques through ABCA1 and combine with cholesterol-saturated α-HDL particles in the plasma to jointly carry cholesterol to the liver. Furthermore, P12 can also convert α-HDL into nascent preβ-HDL particles, which can more efficiently transport cholesterol in the atherosclerotic plaques to the liver and remove excess cholesterol from the

arteries. Moreover, P12 can alleviate atherosclerosis through anti-inflammatory and antioxidant effects in apoE$^{-/-}$ mice.

Therefore, P12 is a promising candidate peptide for development as a new generation atheroprotective agent for cardiovascular disease. P12 represents a new technical innovation that positions us to respond to the "statins-resistance" without contributing to the associated side effects and mortality epidemics or losing the required mildly and effectively anti-atherosclerotic effect.

Acknowledgements

This work was financially supported by the funding from the National Natural Science Foundation of China (81273440) and (81773564).

Conflict of Interest

The authors declare no conflicts of interest.

Author contributions

S.G. performed the experiments and data processing. L.W., G.B. and B.L. did the peptides identification and modification. C.Z. participated in peptides purification. X.C. and X.O. participated in data statistical analysis. X.O. and S.G. participated in animal studies. X.C. Y.Z. and H.L. did the manuscript reading and correction. J.N. and S.G. conceived, supervised, and funded the work. J.N. and S.G. wrote the paper. All authors reviewed the manuscript.

Declaration of transparency and scientific rigour

This Declaration acknowledges that this paper adheres to the principles for transparent reporting and scientific rigour of preclinical research as stated in the BJP guidelines for Design & Analysis, Immunoblotting and Immunochemistry, and Animal Experimentation and as recommended by funding agencies, publishers, and other organizations engaged with supporting research.

ORCID

Sanhu Gou https://orcid.org/0000-0003-3231-7427

References

Alexander, S. P. H., Christopoulos, A., Davenport, A. P., Kelly, E., Marrion, N. V., Peters, J. A., … Collaborators, C. (2017). The Concise Guide to PHARMACOLOGY 2017/18: G protein-coupled receptors. *British Journal of Pharmacology*, 174(S1), S17–S129. https://doi.org/10.1111/bph.13878

Alexander, S. P. H., Fabbro, D., Kelly, E., Marrion, N. V., Peters, J. A., Faccenda, E., … Collaborators, C. G. T. P. (2017). The Concise Guide to PHARMACOLOGY 2017/18: Enzymes. *British Journal of Pharmacology*, 174, S272–S359. https://doi.org/10.1111/bph.13877

Alexander, S. P. H., Peters, J. A., Kelly, E., Marrion, N. V., Faccenda, E., Harding, S. D., … Collaborators, C. G. T. P. (2017). The Concise Guide to PHARMACOLOGY 2017/18: Ligand-gated ion channels. *British Journal of Pharmacology*, 174, S130–S159. https://doi.org/10.1111/bph.13879

Alexander, S. P. H., Roberts, R. E., Broughton, B. R. S., Sobey, C. G., George, C. H., Stanford, S. C., … Ahluwalia, A. (2018). Goals and practicalities of immunoblotting and immunohistochemistry: A guide for submission to the British Journal of Pharmacology. British Journal of Pharmacology, 175, 407–411. https://doi.org/10.1111/bph.14112

Amar, M. J., D'Souza, W., Turner, S., Demosky, S., Sviridov, D., Stonik, J., … Remaley, A. T. (2010). 5A apolipoprotein mimetic peptide promotes cholesterol efflux and reduces atherosclerosis in mice. *The Journal of Pharmacology and Experimental Therapeutics,* 334, 634–641. https://doi.org/10.1124/jpet.110.167890

Arakawa, R., Hayashi, M., Remaley, A. T., Brewer, B. H., Yamauchi, Y., & Yokoyama, S. (2004). Phosphorylation and stabilization of ATP binding cassette transporter A1 by synthetic amphiphilic helical peptides. *The Journal of Biological Chemistry,* 279, 6217–6220. https://doi.org/10.1074/jbc.C300553200

Avdulov, N. A., Chochina, S. V., Igbavboa, U., & Wood, W. G. (2000). Cholesterol efflux to high-density lipoproteins and apolipoprotein A-I phosphatidylcholine complexes is inhibited by ethanol: role of apolipoprotein structure and cooperative interaction of phosphatidylcholine and cholesterol. *Biochemistry,* 39, 10599–10606. https://doi.org/10.1021/bi0008534

Beaufils, C., Alexopoulos, C., Petraki, M. P., Tselepis, A. D., Coudevylle, N., Sakarellos–Daitsiotis, M., … Cung, M. T. (2007). Conformational study of new amphipathic alpha-helical peptide models of apoA-I as potential atheroprotective agents. *Biopolymers*, 88, 362–372. https://doi.org/10.1002/bip.20651

Carballo-Jane, E., Chen, Z., O'Neill, E., Wang, J., Burton, C., Chang, C. H., … Bianchi, E. (2010). ApoA-I mimetic peptides promote pre-beta HDL formation in vivo causing remodeling of HDL and triglyceride accumulation at higher dose. *Bioorganic & Medicinal Chemistry,* 18, 8669–8678. https://doi.org/10.1016/j.bmc.2010.09.074

Chapman, M. J., Orsoni, A., Robillard, P., Therond, P., & Giral, P. (2018). Duality of statin action on lipoprotein subpopulations in the mixed dyslipidemia of metabolic syndrome: Quantity vs quality over time and implication of CETP. *Journal of Clinical Lipidology,* 12, 784–800. https://doi.org/10.1016/j.jacl.2018.02.001

Chroni, A., Koukos, G., Duka, A., & Zannis, V. I. (2007). The carboxy-terminal region of apoA-I is required for the ABCA1-dependent formation of alpha-HDL but not prebeta-HDL particles in vivo. *Biochemistry*, 46, 5697–5708. https://doi.org/10.1021/bi602354t

Chroni, A., Liu, T., Gorshkova, I., Kan, H. Y., Uehara, Y., Von Eckardstein, A., & Zannis, V. I. (2003). The central helices of ApoA-I can promote ATP-binding cassette transporter A1 (ABCA1)-mediated lipid efflux-Amino acid residues 220–231 of the wild-type ApoA-I are required for lipid efflux in vitro and high density lipoprotein formation in vivo. *Journal of Biological Chemistry,* 278, 6719–6730. https://doi.org/10.1074/jbc.M205232200

Curtis, M. J., Alexander, S., Cirino, G., Docherty, J. R., George, C. H., Giembycz, M. A., … Ahluwalia, A. (2018). Experimental design and analysis and their reporting II: updated and simplified guidance for authors and peer reviewers. *British Journal of Pharmacology,* 175, 987–993. https://doi.org/10.1111/bph.14153

D'Souza, W., Stonik, J. A., Murphy, A., Demosky, S. J., Sethi, A. A., Moore, X. L., … Sviridov, D. (2010). Structure/function relationships of apolipoprotein a-I mimetic peptides: implications for antiatherogenic activities of high-density lipoprotein. *Circulation Research,* 107, 217–227. https://doi.org/10.1161/CIRCRESAHA.110.216507

Datta, G., Chaddha, M., Hama, S., Navab, M., Fogelman, A. M., Garber, D. W., … Anantharamaiah, G. M. (2001). Effects of increasing hydrophobicity on the physical-chemical and biological properties of a class A amphipathic helical peptide. *Journal of Lipid Research,* 42, 1096–1104.

Fisher, E. A., Feig, J. E., Hewing, B., Hazen, S. L., & Smith, J. D. (2012). High-density lipoprotein function, dysfunction, and reverse cholesterol transport. *Arteriosclerosis, Thrombosis, and Vascular Biology,* 32, 2813–2820. https://doi.org/10.1161/ATVBAHA.112.300133.

Getz, G. S., & Reardon, C. A. (2011). Apolipoprotein A-I and A-I mimetic peptides: a role in atherosclerosis. *Journal of Inflammation Research,* 4, 83–92. https://doi.org/10.2147/JIR.S12983

Harding, S. D., Sharman, J. L., Faccenda, E., Southan, C., Pawson, A. J., Ireland, S., … NC-IUPHAR (2018). The IUPHAR/BPS Guide to PHARMACOLOGY in 2018: updates and expansion to encompass the new guide to Immunopharmacology. *Nucleic Acids Research*, 46, D1091–D1106. https://doi.org/10.1093/nar/gkx1121

Hafiane, A., & Genest, J. (2015). High density lipoproteins: Measurement techniques and potential biomarkers of cardiovascular risk. *BBA Clinical,* 3, 175–188.

https://doi.org/10.1016/j.bbacli.2015.01.005

Ingenito, R., Burton, C., Langella, A., Chen, X., Zytko, K., Pessi, A., … Bianchi, E. (2010). Novel potent apoA-I peptide mimetics that stimulate cholesterol efflux and pre-beta particle formation in vitro. *Bioorganic & Medicinal Chemistry Letters,* 20, 236–239. https://doi.org/10.1016/j.bmcl.2009.10.128

Islam, R. M., Pourmousa, M., Sviridov, D., Gordon, S. M., Neufeld, E. B., Freeman, L. A., … Remaley, A. T. (2018). Structural properties of apolipoprotein A-I mimetic peptides that promote ABCA1-dependent cholesterol efflux. *Scientific Reports,* 8, 2956. https://doi.org/10.1038/s41598-018-20965-2

Jin, X. T., Sviridov, D., Liu, Y., Vaisman, B., Addadi, L., Remaley, A. T., & Kruth, H. S. (2016). ABCA1 (ATP-Binding Cassette Transporter A1) mediates ApoA-I (Apolipoprotein A-I) and ApoA-I mimetic peptide mobilization of extracellular cholesterol microdomains deposited by macrophages. *Arteriosclerosis Thrombosis and Vascular Biology,* 36, 2283–2291. https://doi.org/10.1161/ATVBAHA.116.308334

Khera, A. V., & Rader, D. J. (2010). Future therapeutic directions in reverse cholesterol transport. *Current Atherosclerosis Reports*, 12, 73–81. https://doi.org/10.1007/s11883-009-0080-0

Kilkenny, C., Browne, W., Cuthill, I. C., Emerson, M., & Altman, D. G. (2010). Animal research: reporting in vivo experiments: the ARRIVE guidelines. *British Journal of Pharmacology,* 160, 1577–1579. https://doi.org/10.1038/jcbfm.2010.220

Leman, L. J., Maryanoff, B. E., & Ghadiri, M. R. (2014). Molecules That Mimic

Apolipoprotein A-I: Potential Agents for Treating Atherosclerosis. *Journal of Medicinal Chemistry,* 57, 2169–2196. https://doi.org/10.1021/jm4005847

Lewis, G. F., & Rader, D. J. (2005). New insights into the regulation of HDL metabolism and reverse cholesterol transport. *Circulation Research,* 96, 1221–1232. https://doi.org/10.1161/01.RES.0000170946.56981.5c

Martinez, L. O., Agerholm-Larsen, B., Wang, N., Chen, W., & Tall, A. R. (2003). Phosphorylation of a pest sequence in ABCA1 promotes calpain degradation and is reversed by ApoA-I. *The Journal of biological chemistry,* 278, 37368–37374. https://doi.org/10.1074/jbc.M307161200

Mei, X. H., & Atkinson, D. (2015). Lipid-free Apolipoprotein A-I Structure: Insights into HDL Formation and Atherosclerosis Development. *Archives of Medical Research,* 46, 351–360. https://doi.org/10.1016/j.arcmed.2015.05.012

Natarajan, P., Forte, T. M., Chu, B., Phillips, M. C., Oram, J. F., & Bielicki, J. K. (2004). Identification of an apolipoprotein A-I structural element that mediates cellular cholesterol efflux and stabilizes ATP binding cassette transporter A1. *The Journal of Biological Chemistry*, 279, 24044–24052. https://doi.org/10.1074/jbc.M400561200

Navab, M., Anantharamaiah, G. M., Hama, S., Garber, D. W., Chaddha, M., Hough, G., … Fogelman, A. M. (2002). Oral administration of an ApoA-I mimetic Peptide synthesized from D-amino acids dramatically reduces atherosclerosis in mice independent of plasma cholesterol. *Circulation,* 105, 290–292. https://doi.org/10.1161/hc0302.103711

Navab, M., Reddy, S. T., Anantharamaiah, G. M., Imaizumi, S., Hough, G., Hama, S., &

Fogelman, A. M. (2011). Intestine may be a major site of action for the apoA-I mimetic peptide 4F whether administered subcutaneously or orally. *Journal of Lipid Research,* 52, 1200–1210. https://doi.org/10.1194/jlr.M013144

Ohashi, R., Mu, H., Wang, X., Yao, Q., & Chen, C. (2005). Reverse cholesterol transport and cholesterol efflux in atherosclerosis. *QJM: An International Journal of Medicine,* 98, 845–856. https://doi.org/10.1093/qjmed/hci136

Osei-Hwedieh, D. O., Amar, M., Sviridov, D., & Remaley, A. T. (2011). Apolipoprotein mimetic peptides: Mechanisms of action as anti-atherogenic agents. *Pharmacology & Therapeutics*, 130, 83–91. https://doi.org/10.1016/j.pharmthera.2010.12.003

Palgunachari, M. N., Mishra, V. K., LundKatz, S., Phillips, M. C., Adeyeye, S. O., Alluri, S., … Segrest, J. P. (1996). Only the two end helixes of eight tandem amphipathic helical domains of human apo A-I have significant lipid affinity- Implications for HDL assembly. *Arteriosclerosis Thrombosis and Vascular Biology,* 16, 328–338. https://doi.org/10.1161/01.ATV.16.2.328

Panagotopulos, S. E., Witting, S. R., Horace, E. M., Hui, D. Y., Maiorano, J. N., & Davidson, W. S. (2002). The role of apolipoprotein A-I helix 10 in apolipoprotein-mediated cholesterol efflux via the ATP-binding cassette transporter ABCA1. *Journal of Biological Chemistry,* 277, 39477–39484. https://doi.org/10.1074/jbc.M207005200

Reddy, S. T., Navab, M., Anantharamaiah, G. M., & Fogelman, A. M. (2014). Searching for a successful HDL-based treatment strategy. *Biochimica et Biophysica Acta,* 1841, 162–167. https://doi.org/10.1016/j.bbalip.2013.10.012

Shimizu. T., Tanigawa, H., Miura, S., Kuwano, T., Takata, K., Suematsu, Y., … Saku, K. (2015). Newly developed apolipoprotein A–I mimetic peptide promotes macrophage reverse cholesterol transport in vivo. *International Journal of Cardiology,* 192, 82–88. https://doi.org/10.1016/j.ijcard.2015.05.012

Stoekenbroek, R. M., Stroes, E. S., & Hovingh, G. K. (2015). ApoA-I mimetics. *Handbook of Experimental Pharmacology*, 224, 631–648. https://doi.org/10.1007/978-3-319-09665-0_21

Sviridov, D. O., Andrianov, A. M., Anishchenko, I. V., Stonik, J. A., Amar, M. J., Turner, S., & Remaley, A. T. (2013). Hydrophobic amino acids in the hinge region of the 5A apolipoprotein mimetic peptide are essential for promoting cholesterol efflux by the ABCA1 transporter. *The Journal of Pharmacology and Experimental Therapeutics,* 344, 50–58. https://doi.org/10.1124/jpet.112.198143

Tsompanidi, E. M., Brinkmeier, M. S., Fotiadou, E. H., Giakoumi, S. M., & Kypreos, K. E. (2010). HDL biogenesis and functions: role of HDL quality and quantity in atherosclerosis. *Atherosclerosis,* 208, 3–9. https://doi.org/10.1016/j.atherosclerosis.2009.05.034

Uehara, Y., Ando, S., Yahiro, E., Oniki, K., Ayaori, M., Abe, S., … Saku, K. (2013). FAMP, a novel apoA-I mimetic peptide, suppresses aortic plaque formation through promotion of biological HDL function in ApoE-deficient mice. *Journal of the American Heart Association,* 2, e000048. https://doi.org/10.1161/JAHA.113.000048

Ushasri, C., Jaipal, K., Srinivas, G., Avinash Raj, T., Mahesh, K. J., Giribabu, L., … Pande,

G. (2014). Synthesis and functional characterization of a fluorescent peptide probe for noninvasive imaging of collagen in live tissues. *Experimental Cell Research*, 327, 91–101. https://doi.org/10.1016/j.yexcr.2014.05.005

Van Lenten, B. J., Wagner, A. C., Anantharamaiah, G. M., Navab, M., Reddy, S. T., Buga, G. M., & Fogelman, A. M. (2009). Apolipoprotein A-I mimetic peptides. *Current Atherosclerosis Reports,* 11, 52–57. https://doi.org/10.1007/s11883-009-0008–8

Wool, G. D., Reardon, C. A., & Getz, G. S. (2014). Mimetic peptides of human apoA-I helix 10 get together to lower lipids and ameliorate atherosclerosis: is the action in the gut? *Journal of Lipid Research,* 55, 1983–1985. https://doi.org/10.1194/jlr.E053538

Xie, Q., Zhao, S. P., & Li, F. (2010). D-4F, an apolipoprotein A-I mimetic peptide, promotes cholesterol efflux from macrophages via ATP-binding cassette transporter A1. *The Tohoku Journal of Experimental Medicine,* 220, 223–228. https://doi.org/10.1620/tjem.220.223

Yao, X., Gordon, E. M., Barochia, A. V., Remaley, A. T., & Levine, S. J. (2016). The a's have it: developing apolipoprotein A-I mimetic peptides into a novel treatment for asthma. *Chest,* 150, 283–288. https://doi.org/10.1016/j.chest.2016.05.035

Zhang, M., He, J., Jiang, C., Zhang, W., Yang, Y., Wang, Z., & Liu, J. (2017). Plaque-hyaluronidase-responsive high-density-lipoprotein-mimetic nanoparticles for multistage intimal-macrophage-targeted drug delivery and enhanced anti-atherosclerotic therapy. *International Journal of Nanomedicine,* 12, 533–558. https://doi.org/10.2147/IJN.S124252

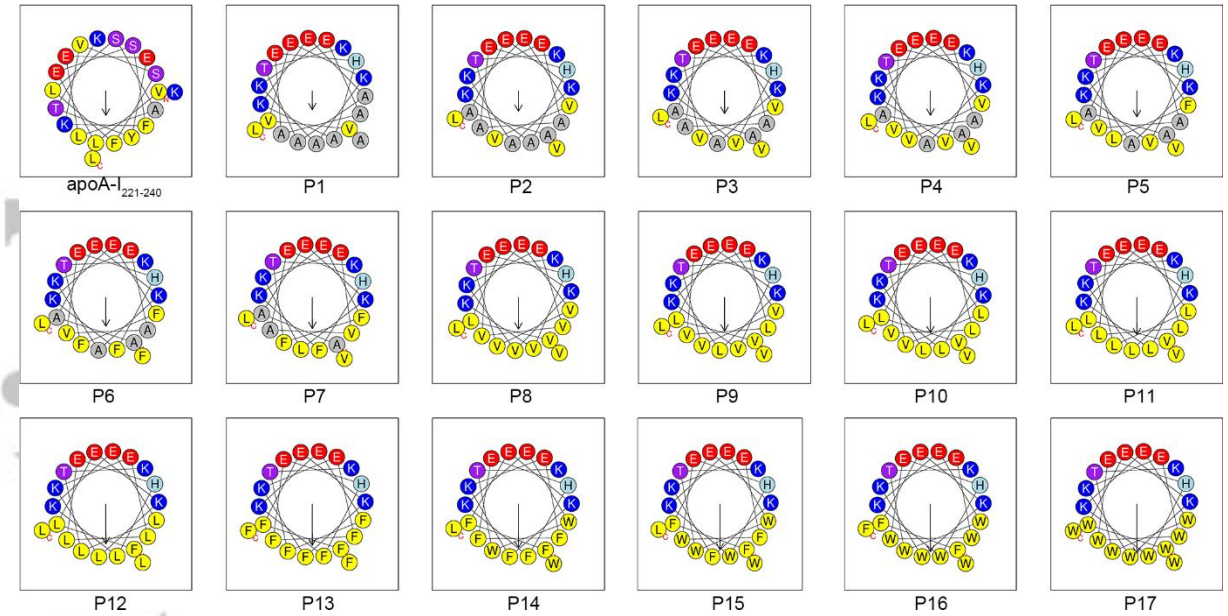

FIGURE 1 The designed peptides (P1–P17) with cholesterol efflux activities possess an amphipathic α-helix structure (figures were exported from HeliQuest online software [https://heliquest.ipmc.cnrs.fr/]). The design strategy was as follow: First, the hydrophobic amino acids on the hydrophilic surface of apoA-$I_{221–240}$ were replaced with hydrophilic amino acids, and the hydrophilic amino acids on the hydrophobic surface of apoA-$I_{221–240}$ were replaced with hydrophobic amino acids. Subsequently, to facilitate the study of the effect of hydrophobicity on the amphiphilic apoA-I mimetic peptides, the substituted amino acids on the hydrophilic surface were fixed, and the hydrophobic amino acids on the hydrophobic surface were gradually replaced with more hydrophobic amino acids. The difference in the hydrophobicity value between two adjacent numbered peptides was approximately 0.05.

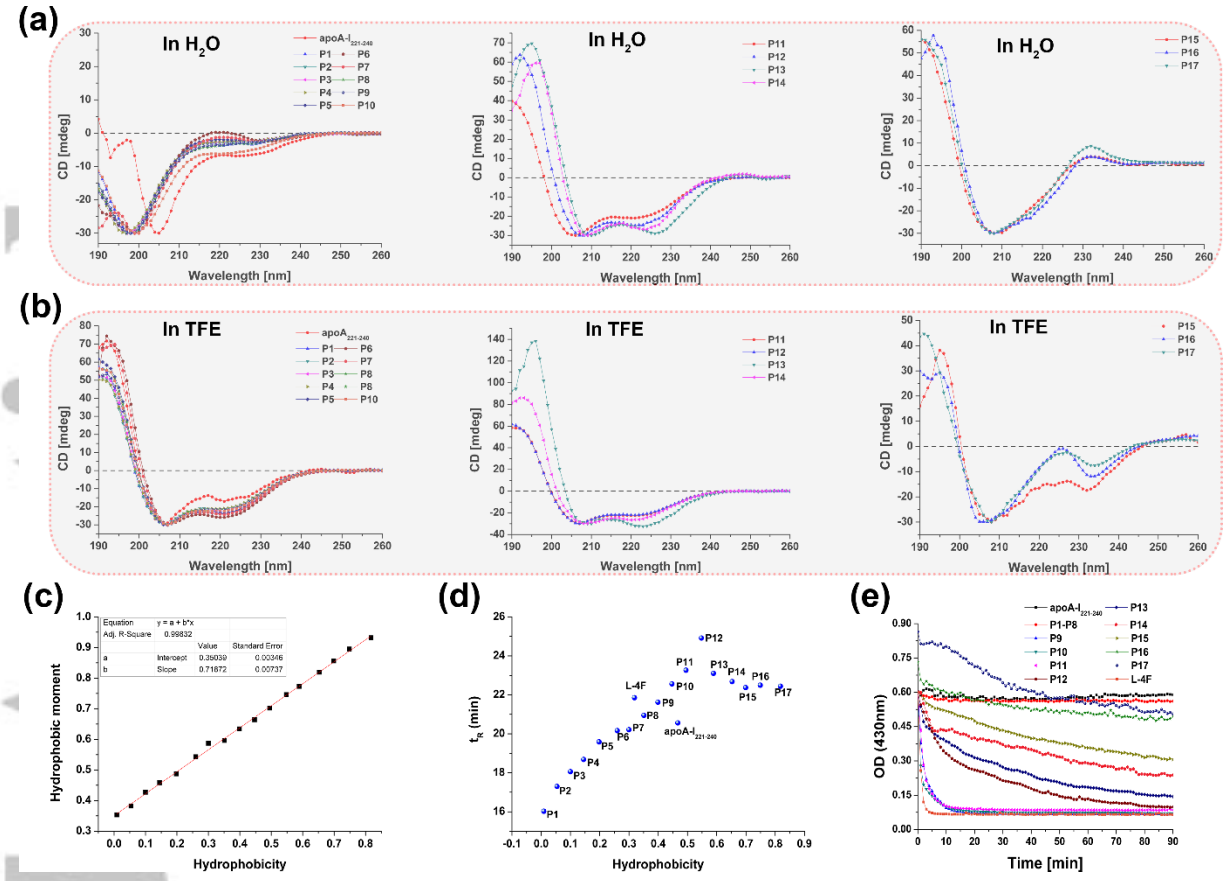

FIGURE 2 Characterization of circular dichroism (CD) spectroscopy, hydrophobicity, t_R, and lipid affinity of the new peptides. (a) CD of apoA-$I_{221–240}$ and P1–P17 in H_2O and (b) in 50% TFE. P11–P14 always maintained an α-helical structure in aqueous and simulated biofilm environment. (c) Hydrophobicity and hydrophobic moment of P1–P17 have a linear relationship (hydrophobic moment = 0.7187 Hydrophobicity + 0.3504, $R^2 = 0.998$). These data were calculated using HeliQuest online software (https://heliquest.ipmc.cnrs.fr/). (d) Effects of hydrophobicity on t_R as determined using reversed-phase HPLC. As the hydrophobicity increased, t_R of P1–P12 increased gradually, whereas the opposite pattern was observed for P12–P17. (e) Lipid affinity evaluation of the peptides. Dimyristoyl phosphatidylcholine (DMPC) vesicle solubilization is visually presented as changes in the optical density of the mixed system of peptides (50 μM) and DMPC (1 $mg \cdot mL^{-1}$) at 430 nm. DMPC vesicles were solubilized by apoA-$I_{221–240}$, P1–P17, and L-4F. Similar to apoA-$I_{221–240}$, P1–P8 did not solubilize DMPC vesicles. Surprisingly, P9–P11 and L-4F made DMPC vesicles clear within 10 min. P12–P17 gradually and slowly induced DMPC vesicle solubilization. P12 induced DMPC vesicles solubilization within 90 min. P16 and P17 were precipitated in DMPC vesicles, and thus, their absorbance was initially greater than 0.6. t_R, retention time. TFE, trifluoroethanol.

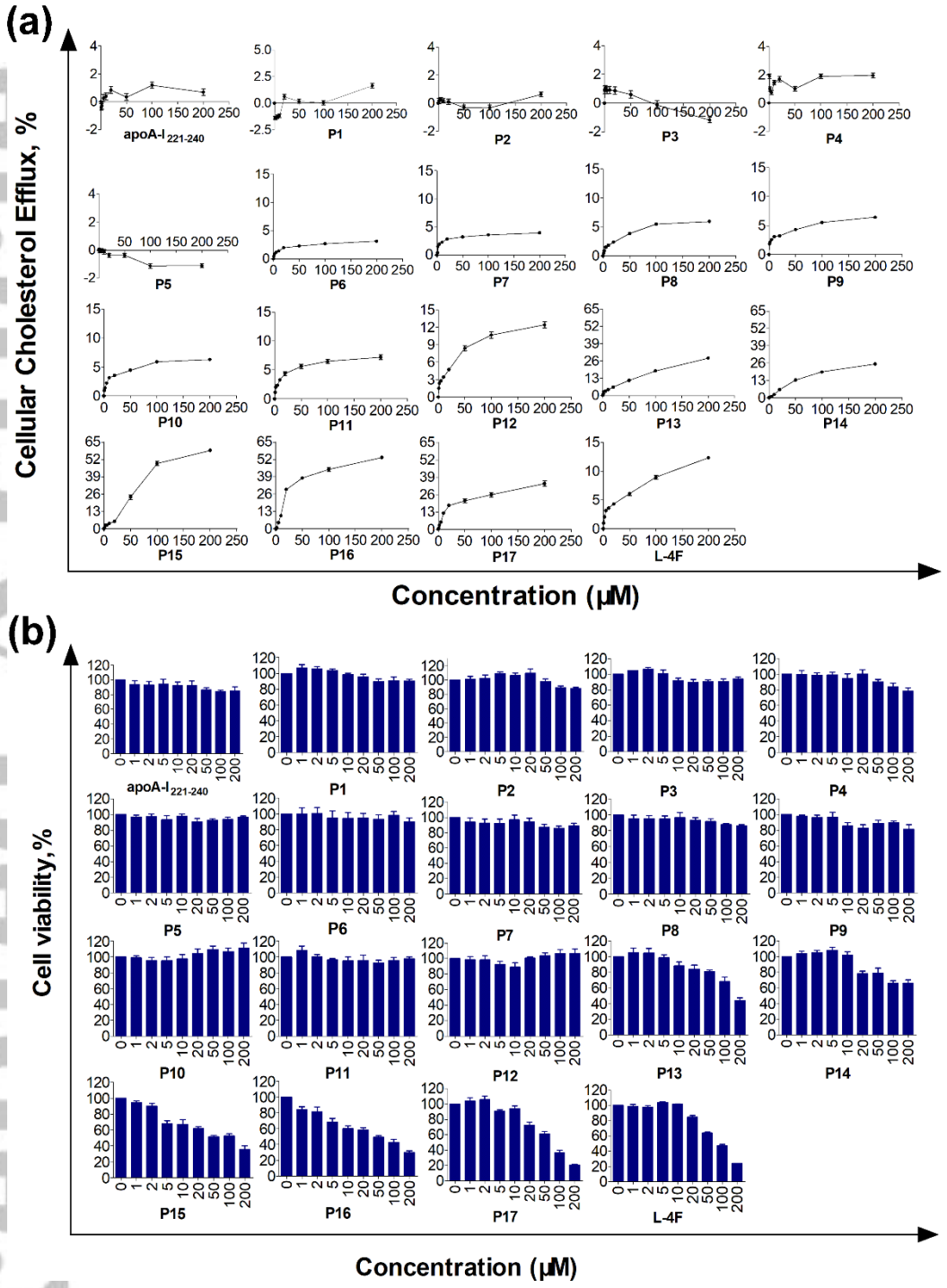

FIGURE 3 Cholesterol efflux activity and cytotoxicity of the parent peptide apoA-$I_{221–240}$, P1–P17, and L-4F in RAW264.7 cells. (a) Cholesterol efflux activity of apoA-I mimetic peptides in RAW264.7 cells after 12 h of treatment. ApoA-$I_{221–240}$ and P1–P5 had no concentration-dependent cholesterol efflux activities. P6–P17 and L-4F had concentration-dependent cholesterol efflux activities. (b) The cytotoxicity of apoA-I mimetic peptides in RAW264.7 cells after 12 h of treatment. ApoA-$I_{221–240}$ and P1–P12 had no cytotoxicity, whereas P13–P17 and L-4F induced obvious cytotoxicity. n = 5. Each experiment was repeated independently five times.

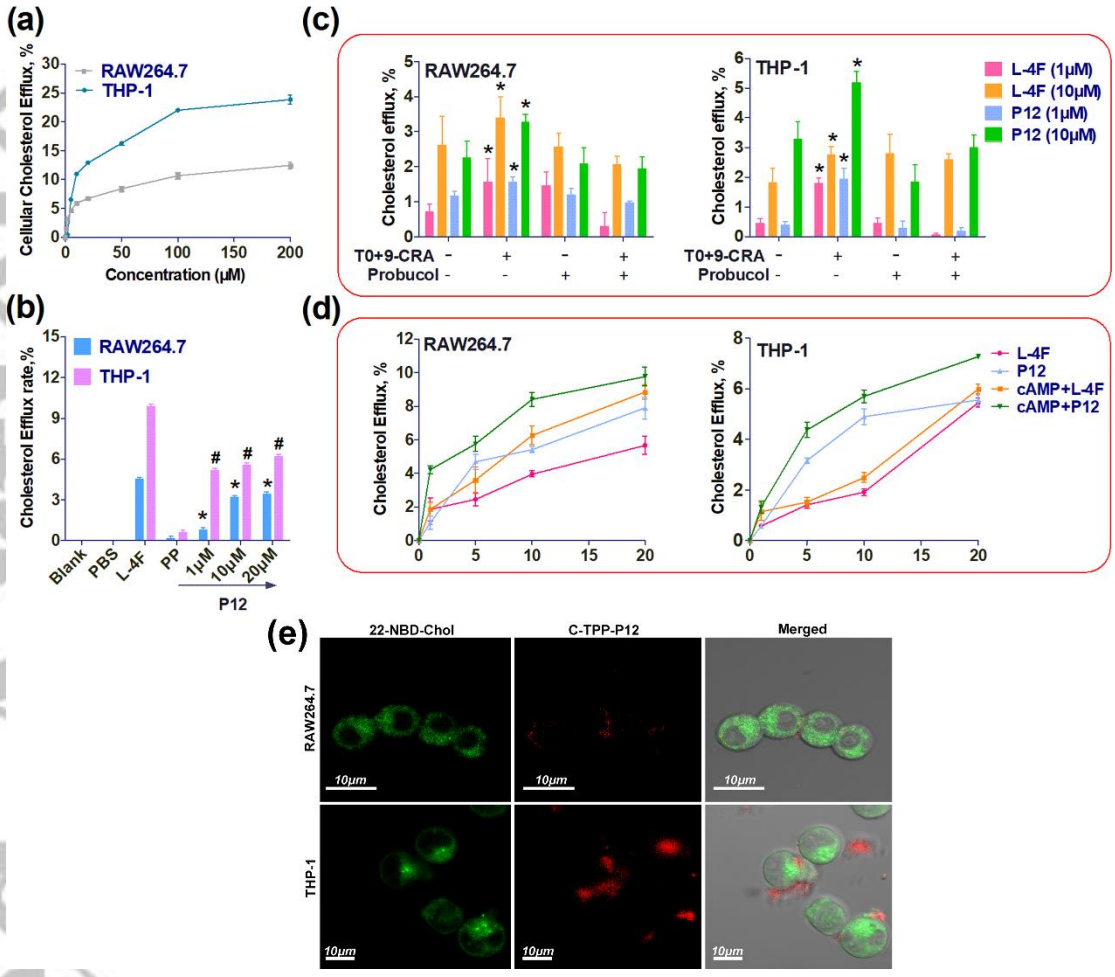

FIGURE 4 Comparison of cholesterol efflux activity of P12 in RAW264.7 and THP-1 cells, ATP-binding cassette transporter A1 (ABCA1)-dependent cellular cholesterol efflux and the action site of 5-(4-carboxyphenyl)-10, 15, 20-triphenylporphyrin (C-TPP)-labeled P12 in macrophages (a) Cholesterol efflux rates induced by P12 in RAW264.7 and THP-1 cells were measured using a multimode reader. (b) Cholesterol efflux induced by P12 (1, 10, and 20 μM) in 22-NBD-cholesterol labeled RAW264.7 and THP-1 were measured using a flow cytometer. Blank represents unlabeled cells using 22-NBD-cholesterol. All peptides were dissolved in PBS. $*P < .05$ significantly different from PP (apoA-$I_{221–240}$) in RAW264.7 cells, $\#P < .05$ significantly different from PP (apoA-$I_{221–240}$) in THP-1 cells. One-way ANOVA followed by Dunnett's post-hoc test. (c) ABCA1-dependent cellular cholesterol efflux induced by 5 μM of 9-cis-retinoic acid (9-CRA) and TO-901317 (TO) for 10 h. To suppress ABCA1, cells were treated with 20 μM probucol for 2 h. $*P < .05$ significantly different from untreated cells by TO and 9-CRA. Student's t-test. (d) ABCA1-dependent cellular cholesterol efflux induced by 0.3 M cAMP 12 h. (e) Laser scanning confocal microscope images of C-TPP-P12 and 22-NBD-cholesterol in RAW264.7 and THP-1 cells. C-TPP-P12 staining was observed outside the cell and on the cell membrane. Membrane C-TPP-P12 staining was stronger in THP-1 cells than in RAW264.7 cells. Each data point represents the mean ± SEM. n = 5. Each experiment was repeated independently five times.

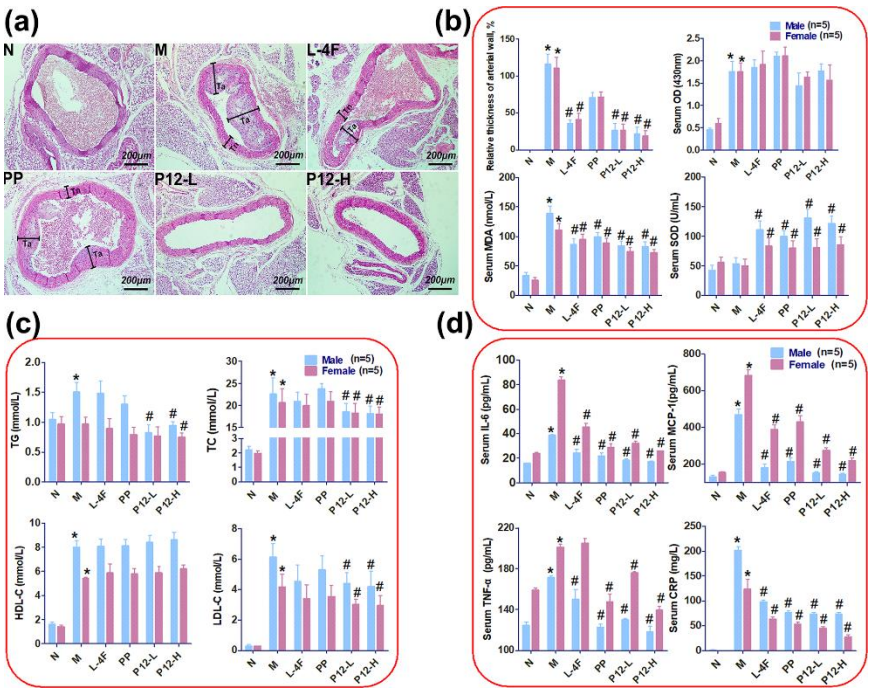

FIGURE 5 The arterial plaques-reducing effect of P12 in apoE$^{-/-}$ mice and relative thickness of arterial wall (%), serum MDA, SOD, lipid (TG, TC, HDL-C, and LDL-C), and inflammatory factor levels (IL-6, MCP-1, TNF-α, and CRP), and serum turbidity (optical density, $OD_{430\ nm}$) in mice. (a) The effects of P12 on atherosclerosis in apoE$^{-/-}$ mice (cross-section of arteries, staining with hematoxylin and eosin, normal thickness of the arterial wall is indicated by black lines and Tn, and abnormal thickness of arterial wall is indicated by black lines and Ta). (b) Effects of P12 on the relative thickness of arterial wall, and serum turbidity, MDA, and SOD levels. Relative thickness of the arterial wall (%) = (Ta − Tn)/Tn × 100%. Five mice were taken from each group, and three samples were taken from each mouse. Serum turbidity was presented as $OD_{430\ nm}$. The relative thickness of arterial wall, serum turbidity, and serum MDA levels was decreased by P12 treatment, whereas serum SOD level was increased. (c) Effects of P12 on serum lipid levels (TG, TC, HDL-C, and LDL-C). Serum TG, TC, and LDL-C levels were decreased by P12. (d) Effects of P12 on serum inflammatory factor levels (IL-6, MCP-1, TNF-α, and CRP). Serum IL-6, MCP-1, TNF-α, and CRP levels were decreased by P12 treatment in apoE$^{-/-}$ mice. Each data point represents the mean ± SEM. $^{*}P < .05$, significantly different from normal control. $^{\#}P < .05$, significantly different from model control. One-way ANOVA followed by Dunnett's post-hoc test. n = 10, including 5 male and 5 female mice. N, normal control group. M, model control group. L-4F, L-4F (10 mg·kg^{-1}) treatment group. PP, parent peptide apoA-$I_{221–240}$ (10 mg·kg^{-1}) treatment group. P12-L and -H indicate treatment with 10 and 20 mg·kg^{-1} P12, respectively. MDA, malondialdehyde. SOD, superoxide dismutase. TG, triacylglycerol. TC, total cholesterol. MCP-1, monocyte chemoattractant protein-1. CRP, C-reactive protein.

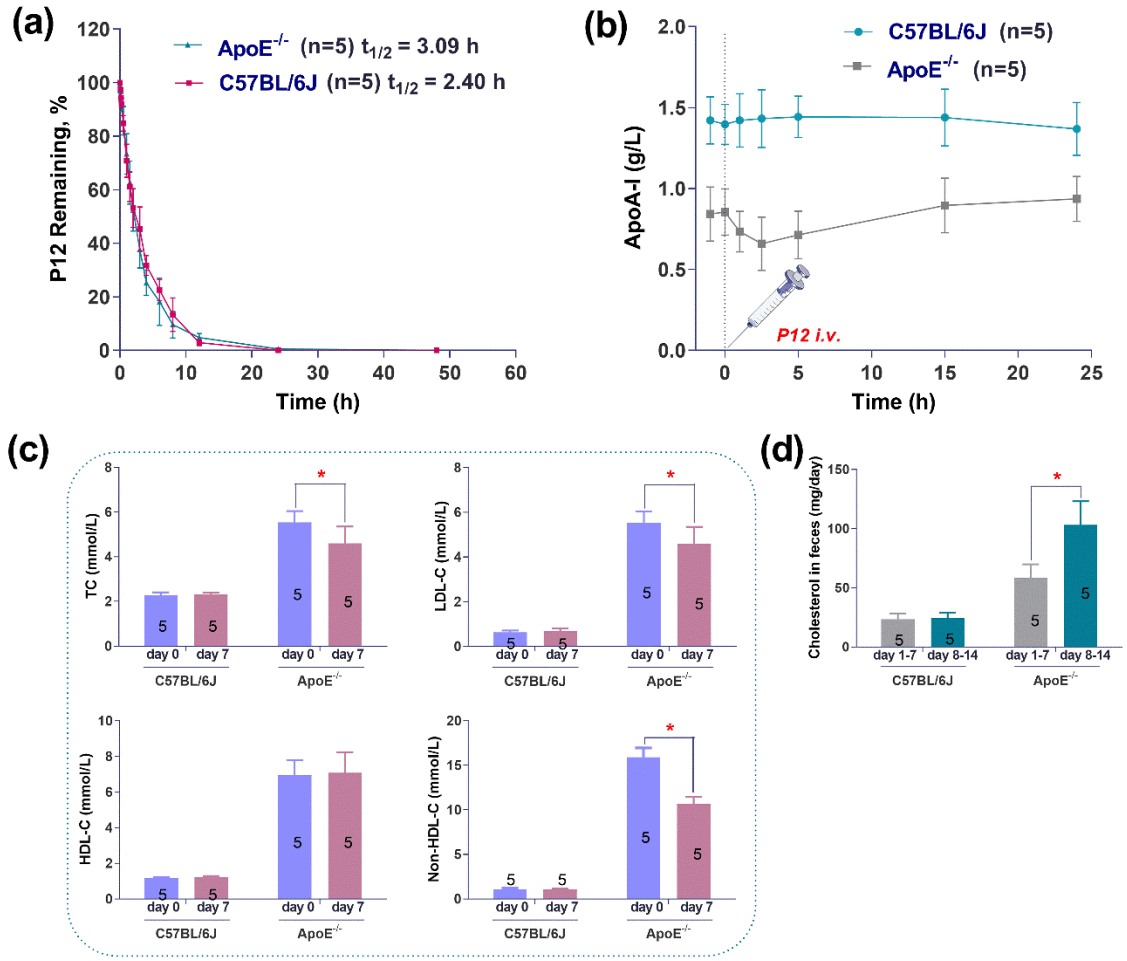

FIGURE 6 Half-life of P12, and effects of P12 on plasm apoA-I levels, blood lipid levels, and cholesterol excretion. (a) Plasma clearance and half-life ($t_{1/2}$) of P12 (10 mg·kg^{-1} i.v.). The plasma $t_{1/2}$ of P12 was 3.09 h in apoE$^{-/-}$ and 2.40 h in C57BL/6J mice. P12 was cleared with first-order kinetics in both mouse strains. (b) Effect of P12 (10 mg·kg^{-1} i.v.) on plasma apoA-I levels. P12 slowly increased plasma apoA-I levels in apoE$^{-/-}$ mice within 24 h, whereas it had no effect on plasma apoA-I levels in C57BL/6J mice. (c) Effects of 1 week of P12 treatment on serum total cholesterol (TC), LDL-C, HDL-C, and non-HDL-C levels in apoE$^{-/-}$ and normal C57BL/6J mice. Day 0, the measurement was conducted one day before the experiment began. Day 7, the measurement was conducted on the seventh day. *$P < .05$, significantly different from blood lipid levels in apoE$^{-/-}$ mice at day 0. Student's t-test. (d) Effect of 2 weeks of P12 treatment on cholesterol excretion. *$P < .05$, significantly different from cholesterol excretion of apoE$^{-/-}$ mice at day 1–7. Student's t-test. Data are presented as the mean ± SEM. n = 5. Each experiment was repeated independently five times.

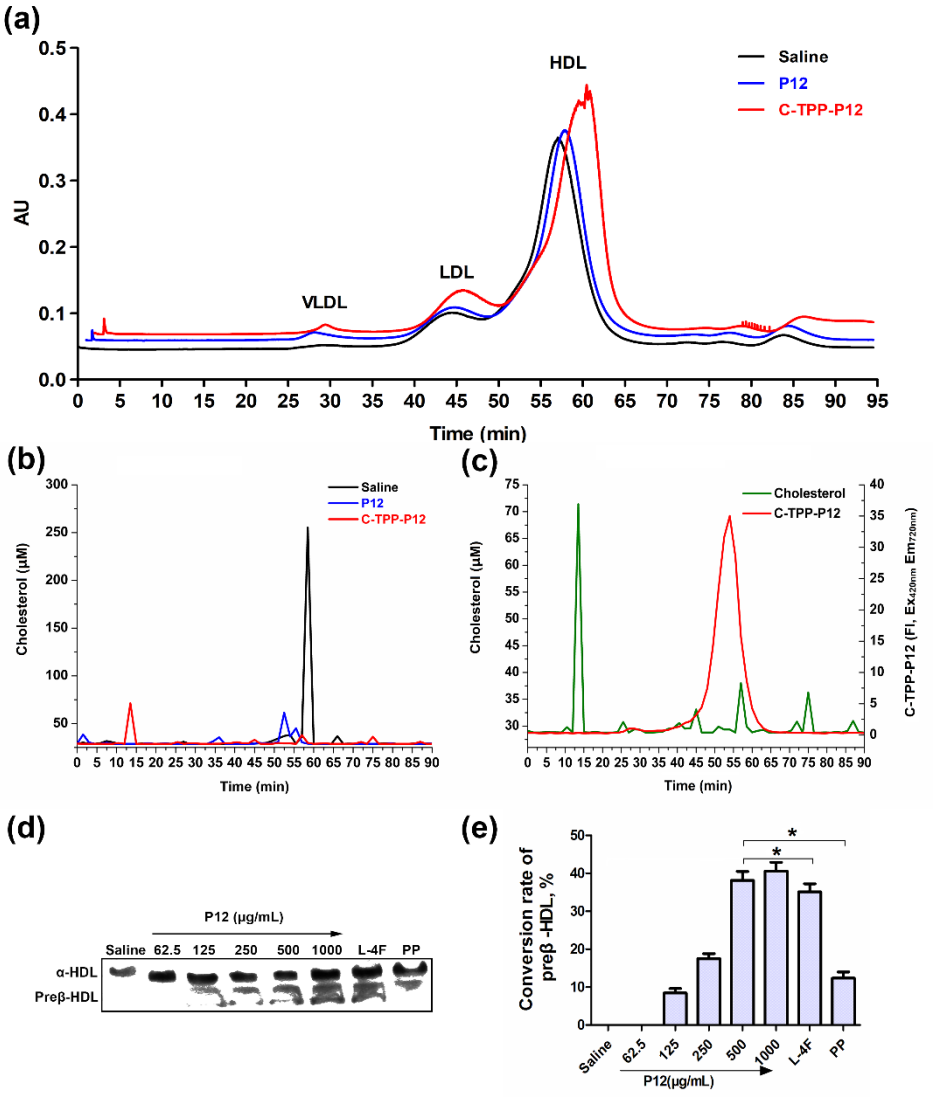

FIGURE 7 The separation of lipoproteins in the plasma of mice after co-incubation with P12. (a) The separation chromatogram of lipoproteins obtained using size exclusion chromatography (Superose 6 column, 10 × 1000 mm) after incubation with P12 (0.25 mg·mL^{-1}, blue line), 5-(4-carboxyphenyl)-10, 15, 20-triphenylporphyrin (C-TPP)-P12 (0.25 mg·mL^{-1}, red line) and saline (blank control, black line) at 280 nm. (b) Size exclusion chromatography fractions (1.5 min·fraction^{-1}). The relative cholesterol content of each fraction measured using a cholesterol kit. (c) C-TPP-P12 and cholesterol were measured in each size exclusion chromatography fraction after co-incubation of C-TPP-P12 with plasma. (d) The native polyacrylamide gel-separated plasma lipoprotein after co-incubation with P12 (62.5–1000 μg·mL^{-1}), L-4F (500 μg·mL^{-1}), and parent peptide apoA-I$_{221–240}$ (PP, 500 μg·mL^{-1}). (e) Western blotting band after analyzing the gray value using Photoshop and calculating the conversion rates of preβ-HDL induced by the peptides. n = 5. Each experiment was repeated independently five times. Each data point represents the mean ± SEM. *$P < .05$, significantly different from P12 (500 μg·mL^{-1}). One-way ANOVA followed by Dunnett's post-hoc test.

TABLE 1 Amino acid sequences and α-helix content of human apolipoprotein A1 (apoA-I) fragments and apoA-I mimetic peptides.

Peptide	Sequence	α-helix content, %	
		in H_2O	in 50%TFE
apoA-$I_{221–240}$	H-VLESFKVSFLSALEEYTKKL-OH	18.97	46.62
P1	H-V**V**EK**A**AK**E**A**A**E**H**AKE**AA**TK**A**L-OH	10.11	65.87
P2	H-**AA**EK**A**AK**E**A**A**E**H**AKE**VV**TK**V**L-OH	8.15	59.60
P3	H-**AA**EK**A**AK**E**A**A**E**H**V**K**E**VV**TK**V**L-OH	7.11	61.11
P4	H-**AA**EK**A**AK**E**AVE**H**V**K**E**VV**TK**V**L-OH	6.87	59.25
P5	H-**AA**EK**A**AK**E**AVE**H**V**K**E**FL**TK**V**L-OH	5.67	67.23
P6	H-**AA**EK**A**AK**E**AVE**H**F**K**E**FF**TK**F**L-OH	-0.41	72.80
P7	H-**AA**EK**L**K**E**VAE**H**F**K**E**FF**TK**V**L-OH	3.55	68.64
P8	H-VLEK**V**K**E**VVE**H**V**K**E**VV**TK**V**L-OH	9.71	61.36
P9	H-VLEK**L**K**E**LVE**H**V**K**E**VV**TK**V**L-OH	9.24	61.45
P10	H-VLEK**L**K**E**LVE**H**L**K**E**LV**TK**V**L-OH	17.42	63.11
P11	H-VLEK**L**K**E**LLE**H**L**K**E**LL**TK**V**L-OH	59.23	63.85
P12	H-**F**LEK**L**K**E**LLE**H**L**K**E**LL**TK**L**L-OH	70.23	62.34
P13	H-**FF**EK**F**K**E**FFE**H**F**K**E**FF**TK**FF**-OH	75.16	91.96
P14	H-**FF**EK**F**K**E**FFE**H**F**K**E**WW**TK**W**L-OH	75.84	74.80
P15	H-**FF**EK**F**K**E**F**W**E**H**W**K**E**WW**TK**W**L-OH	30.27	42.62
P16	H-**FF**EK**W**K**E**W**W**E**H**W**K**E**WW**TK**WF**-OH	40.01	15.36

P17	H-**WW**E**K**W**K**E**WW**E**H**W**K**E**WW**TK**WW**-OH	30.78	16.41
L-4F[a]	Ac-DWFKAFYDKVAEKFKEAF-NH_2	52.77	66.25

a, L-4F was used as a positive control. The bold letters are the replaced amino acids compared with the parent peptide apoA-$I_{221–240}$. The letters in the box represent the unchanged amino acid residues of the hydrophilic face. TFE, Trifluoroethanol.

TABLE 2 The cholesterol efflux activity, cytotoxicity, and hemolytic effects of human apolipoprotein A1 (apoA-I) fragments and apoA-I mimetic peptides.

Peptide	CE, % (10μM), 12h	Cell viability, % (100μM), 12h	Hemolysis, % (200μM), 1h
apoA-$I_{221–240}$	0.38 ± 0.24	84.27 ± 1.91	1.34 ± 0.66
P1	–1.17 ± 0.17	90.65 ± 4.93	–1.84 ± 0.26
P2	0.18 ± 0.13	89.40 ± 2.48	1.25 ± 0.65
P3	0.91 ± 0.25	90.43 ± 3.40	–0.28 ± 0.49
P4	1.45 ± 0.15	84.20 ± 4.40	0.99 ± 0.66
P5	–0.12 ± 0.17	93.98 ± 2.71	1.20 ± 0.78
P6	1.41 ± 0.11	97.80 ± 5.20	–1.78 ± 0.17
P7	2.29 ± 0.17	85.60 ± 3.20	–0.74 ± 0.41
P8	1.82 ± 0.13	87.50 ± 1.60	–0.52 ± 0.49
P9	3.09 ± 0.12	89.40 ± 2.20	–0.37 ± 0.87
P10	3.14 ± 0.22	106.70 ± 4.80	–0.41 ± 0.60
P11	3.30 ± 0.26	95.30 ± 3.90	1.64 ± 0.78
P12	3.39 ± 0.28	106.77 ± 5.07	1.71 ± 0.73
P13	4.33 ± 0.38	68.20 ± 5.30	1.99 ± 0.67
P14	2.49 ± 0.44	66.00 ± 3.00	2.63 ± 0.70
P15	4.01 ± 0.31	52.41 ± 3.16	7.06 ± 0.86
P16	9.75 ± 0.97	42.61 ± 4.00	5.94 ± 0.58

P17	12.23 ± 0.63	36.62 ± 3.40	7.86 ± 0.64
L-4F[a]	3.61 ± 0.19	47.07 ± 1.89	2.10 ± 0.48

Data are presented as the mean ± SEM. More detailed data are presented in the supplementary materials. a, L-4F was used as a positive control. CE, cholesterol efflux.

A novel apoA-I mimetic peptide suppresses atherosclerosis by promoting physiological HDL function in apoE−/− mice

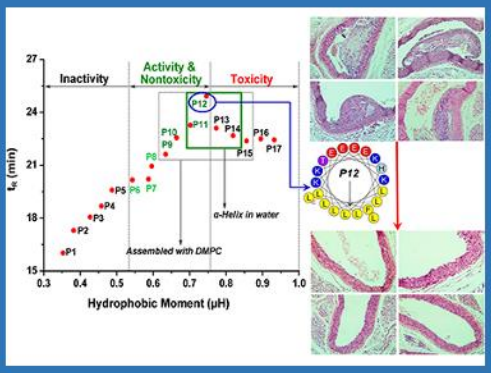

Apolipoprotein A-I (apoA-1) mimetic peptides have emerged as potentially useful treatment options for atherosclerosis. In this study, we designed a series of peptides based on amino acids 221–240 of apoA-I, which contains the ABCA1 binding domain, and assessed the effects on lipid levels in vitro and in vivo. One peptide, dubbed P12, exhibited both strong ABCA1-dependent cholesterol efflux activity and low cytotoxicity in macrophages. In apoE−/− mice, this peptide was demonstrated to coordinately work with HDL to induce reverse cholesterol transport. Those focused on the development of P12 for treatments atherosclerosis and other diseases associated with high cholesterol levels.

Gou, et al. *Br. J. Pharmacol.*

BJP British Journal of Pharmacology

Bullet point summaries

- What is already known about this subject

Apolipoprotein A-I (apoA-1) mimetic peptides have emerged as potentially useful treatments for atherosclerosis.

- What this study adds

The contribution of hydrophobicity to the activity of apoA-I mimetic peptide was important.

The optimal apoA-I mimetic peptide (P12) was identified.

- What is the clinical significance

P12 is a promising candidate peptide for development as a new generation atheroprotective agent for cardiovascular disease.